https://doi.org/10.5194/egusphere-2025-2186
Preprint. Discussion started: 28 May 2025

A Transformer-based agent model of GEOS-Chem v14.2.2 for informative prediction of $PM_{2.5}$ and O_3 levels to future emission scenarios: TGEOS v1.0

Dehao Li[1], Jianbing Jin*[1], Guoqiang Wang[2], Mijie Pang[3], and Hong Liao*[1]

[1]State Key Laboratory of Climate System Prediction and Risk Management, Jiangsu Key Laboratory of Atmospheric Environment Monitoring and Pollution Control, Jiangsu Collaborative Innovation Center of Atmospheric Environment and Equipment Technology, School of Environmental Science and Engineering, Nanjing University of Information Science and Technology, Nanjing, Jiangsu, China
[2]School of Mathematics, Physics and Statistics, Shanghai University of Engineering Science, Shanghai, China
[3]Delft Institute of Applied Mathematics, Delft University of Technology, Delft, the Netherlands

Correspondence: Jianbing Jin (jianbing.jin@nuist.edu.cn) and Hong Liao (hong.liao@nuist.edu.cn)

Abstract. Efficient and informative air quality modeling in future emission scenarios is vital for effective formulation of emission reduction policies. Traditional chemical transport models (CTMs) struggle with the computational demands required for timely predictions. While advanced response surface models (RSMs) were proposed and offered much faster estimates than CTMs, they fall short in providing comprehensive estimates of future air quality due to their simplistic and inflexible structural frameworks. Additionally, current RSMs often have difficulty simultaneously accounting for varying emission variables and the effects of regional transport, which limits their applicability and undermines prediction accuracy. In this study, an informative future air quality prediction model "TGEOS v1.0" based on the Transformer framework is developed as an efficient agent model of GEOS-Chem v14.2.2. TGEOS is able to swiftly and accurately conduct online predictions of probability distributions for $PM_{2.5}$ and O_3 concentrations under future emission scenarios and capture potential extreme pollution events. The model incorporates sectoral emissions of up to 26 distinct species as well as the impacts of regional emissions and meteorology on pollutant concentrations, enhancing its versatility and predictive accuracy. The spatial and probability distributions predicted by TGEOS are in good agreement with GEOS-Chem, with the correlation coefficients for $PM_{2.5}$ and O_3 exceed 0.97 and 0.96, respectively. Notably, TGEOS achieves remarkable computational efficiency, executing one-year predictions in approximately 2.51 seconds. Compared with other machine learning models, TGEOS based on Transformer framework showcases superior performance, underscoring the potential of the Transformer framework in air quality modeling.

1 Introduction

Air pollution constitutes a significant public health emergency due to its detrimental effects on human health, contributing to approximately 6.7 million premature deaths annually (Fuller et al., 2022), particularly in fast developing countries such as China (Lelieveld et al., 2015; Organization et al., 2023). $PM_{2.5}$ and ozone (O_3), recognized as major air pollutants, demonstrate a strong correlation with cardiovascular diseases and all-cause mortality (Al-Kindi et al., 2020). Elevated exposure to these

https://doi.org/10.5194/egusphere-2025-2186
Preprint. Discussion started: 28 May 2025

pollutants considerably exacerbates the public health burden (Bell et al., 2004; Chen et al., 2023a; Wei et al., 2024). $PM_{2.5}$ is a complex pollutant with sources including road dust (Chen et al., 2019), fuel combustion(Bond et al., 2007), and natural sources like wildfires (Burke et al., 2023) and dust storms (Rodríguez and López-Darias, 2024), along with secondary formation through atmospheric reactions (McDuffie et al., 2021). The concentration of ambient $PM_{2.5}$ is influenced by local and ambient emissions (Qiao et al., 2021). Similarly, as a secondary pollutant resulting from photochemical reactions involving various precursors such as nitrogen oxides (NO_x) and volatile organic compounds (VOC_s) (Wang et al., 2017), O_3 concentrations have been shown to be sensitive to both local and regional precursor emissions (Wei et al., 2019; Wang et al., 2021; Gong et al., 2020). $PM_{2.5}$ and ozone pollution has emerged as the central environmental topic in China, with multiple incidences of extreme air pollution occurring in typical areas such as the North China Plain (NCP) and the Yangtze River Delta (YRD) (Silver et al., 2018; Lu et al., 2020a). Focusing on severe $PM_{2.5}$ pollution in China, the Chinese government has launched a series of emission control plans (CSC, 2013, 2018). Although the implementation of effective control policies has resulted in reductions in precursor emissions (Zheng et al., 2021) and the consequent decrease in $PM_{2.5}$ concentrations (Xiao et al., 2021), many air pollution issues still persist. For instance, an increase in domestic surface ozone levels has been observed between 2013 and 2020 (Han et al., 2024), as well as a rebound trend for $PM_{2.5}$ pollution in recent years (Le et al., 2020; Wang et al., 2024). Therefore, it is imperative for China to formulate more holistic and accurate emission control plans to combat air pollution (Wang et al., 2023; Geng et al., 2024). Concurrently, a model with the ability to rapidly and accurately predict air pollutants concentrations under different emission scenarios is in demand for policymakers.

As comprehensive and reliable tools for simulating atmospheric processes (Seinfeld and Pandis, 2016), Chemical Transport Models (CTMs) are widely used to estimate air pollutant levels under different control measures (Zhang et al., 2023). CTMs can provide historical, current and future estimates of various air pollutants, including $PM_{2.5}$ and O_3, by solving mass equations with certain input dataset, e.g. emission and meteorology fields (Seinfeld and Pandis, 2016; Cheng et al., 2021; Zeng et al., 2022), thus bridging the connection between the inputs (emission and meteorology data) and the outputs (concentrations of air pollutants) (Shi et al., 2020; Yan et al., 2021). Therefore, CTMs have been used to investigate the sensitivity of air pollutant concentrations to anthropogenic emissions (Thunis et al., 2021) and meteorological conditions (Shi et al., 2020), as well as to guide the formulation of air quality policies by simulating the air quality response to various emission scenarios (Che et al., 2011; Zhang et al., 2022b, 2023). For example, Zhang et al. (2023) used the Weather Research and Forecasting and Community Multi-scale Air Quality (WRF-CMAQ) model to simulate O_3 concentrations under different VOCs and NO_x emission reduction scenarios in Northeast China to explore effective control strategies for ozone pollution; Zhang et al. (2022b) used the Goddard Earth Observing System with Chemistry model (GEOS-Chem), a CTM with the advantage of incorporating advanced gas-aerosol chemistry and consistently evaluating against atmospheric observations (Lu et al., 2020b; Hu et al., 2017), to evaluate the benefits of different NH_3 emission reduction strategies for $PM_{2.5}$ mitigation in China. Although CTMs demonstrate considerable accuracy in air pollution modeling, they also present notable limitations (Salman et al., 2024), including substantial consumption of computational resources and inefficiencies when conducting long-term simulations over extensive areas or high-resolution grids (Thompson and Selin, 2012). Typically, for GEOS-Chem version 14.2.2, on a computational cluster utilizing 32 cores, a 1-year full-chem nested simulation of China at a resolution of 0.5×0.625 requires approximately

https://doi.org/10.5194/egusphere-2025-2186
Preprint. Discussion started: 28 May 2025

350 hours, and this duration is expected to increase when conducting simulations at finer resolutions or over extended time periods. This limitation makes it impossible for CTMs to meet the needs of policymakers for timely online responses to future air quality under interested scenarios.

To address the computational challenge and efficiently retrieve the nonlinear relationship between emissions and concentrations, data-driven statistical emulators have been proposed to accelerate numerical simulations (Castruccio et al., 2014). A reliable emulator can accurately depict intricate relationships between inputs and outputs, such as from emissions to concentrations. It can also faithfully approximate the fundamental mechanisms of atmospheric models, thereby generating numerical simulations that exhibit a high degree of consistency to the model (Salman et al., 2024). Among all the emulators, Response Surface Model (RSM) is the most widely used method. It is a statistical method developed by the US EPA (EPA, 2006) that uses the maximum likelihood estimation - empirical best linear unbiased predictors (MLE-EBLUPs) technique (Santner et al., 2003) to establish the complex relationships between emission rates of several pollutants and the responses they produce on the pollutant concentrations by fitting response surfaces of the nonlinear system (Box and Draper, 2007), and provide best estimate of the pollutant. When given some unknown emission scenarios, RSM can rapidly retrieve the changes of aimed concentrations without additional CTM simulation involved (Wang et al., 2011). RSM technique has been successfully employed in the response modeling of $PM_{2.5}$ (Wang et al., 2011) and ozone (Xing et al., 2011) to precursor emissions in China for typical regions. Since conventional RSM commonly requires a large number of CTM simulations to fit reliable response surfaces (Xing et al., 2011; Zhao et al., 2015), notable advances focusing on enhancements in both efficiency and accuracy in RSM technology have been achieved (Li et al., 2022). For example, Extended Response Surface Models (ERSMs) (Zhao et al., 2015; Xing et al., 2017) allow for the incorporation of a greater number of variables and geographical regions, improving alignment with independent CTM simulations compared with traditional RSM (Zhao et al., 2015; Xing et al., 2017). Moreover, the polynomial function based RSM (pf-RSM) is capable of quantifying the nonlinear relationships between air pollutant concentrations and precursor emissions by fitting CTM simulations to a series of polynomial functions and mitigating the computational burden through decreasing the number of required CTMs up to 60% (Xing et al., 2018). Recently, many studies have used novel machine learning techniques to accelerate the modeling process of RSM by further reducing the number of required CTMs. For instance, Deep-RSM, developed by Xing et al. (2020) using convolution neural networks (CNN), requires only two CTM cases (i.e., base and control scenarios) to startup the model; Self-adaptive RSM (SA-RSM, Li et al. (2022)) further reduces the number of required CTMs for pf-RSM modeling by employing a stepwise regression method to estimate the coefficients of polynomial functions.

Although existing RSM techniques exhibit more efficiency than traditional CTM in predicting the response of pollutant concentrations to a wide range of emission changes, there are still several issues to be addressed. Firstly, due to the structural limitations that restrict the model from executing multi-target predictions, existing techniques focus mainly on the response of average of the target pollutants over a period of time, such as the monthly average (Huang et al., 2021). However, predicting the singular monthly average of pollutant concentrations may overlook critical variations throughout the month, such as extreme values (Guo et al., 2020; Zhao et al., 2022). Therefore, these approaches fall short in providing a comprehensive evaluation of future pollution states, including the ability to identify potential extreme pollution events under various emission scenar-

https://doi.org/10.5194/egusphere-2025-2186
Preprint. Discussion started: 28 May 2025

ios. Secondly, RSM techniques rely on the polynomial assumption, leading to its disadvantage to cope with high-dimension problems. As the number of input variables increases, the complexity of RSM model grows, necessitating a larger number of samples for accurate fitting (Zhao et al., 2015) and potentially leading to multi-collinearity issues (Xing et al., 2018). This limitation restricts the applicability of RSM to more intricate emission scenarios. Therefore, existing RSM studies have primarily concentrated on emissions of a few major pollutants and the add-up emissions, failing to address air quality response under more detailed scenarios that incorporate sectoral emissions and a broader range of emission species. While ERSM considers emission sectors (Zhao et al., 2015), the inherent limitations of RSM in handling high-dimensional data result in a substantial requirement for CTM samples, thus confining its application to modeling studies in smaller areas. Thirdly, current RSMs e.g. pf-RSM (Xing et al., 2018) and SA-RSM (Li et al., 2022) account for each spatial grid independently while neglect the impact of surrounding emissions, which have been shown to affect local pollutant concentrations (Cheng et al., 2019). While ERSM (Zhao et al., 2015) has considered regional transport of emissions, it requires a substantial number of scenario simulations to ensure the accuracy of the model (Zhao et al., 2015; Xing et al., 2017). For example, modeling for a middle-scale region typically necessitates hundreds of scenarios as support (Zhao et al., 2015). The computational burden significantly limits the application of this technology on a national scale. In summary, given that existing techniques inadequately address the challenges associated with high temporal-resolution prediction, inapplicability of multivariate scenarios, and negligence of emission transport, developing a comprehensive national-level "emission-concentration" predictive model poses a significant challenge.

Machine learning (ML), as a novel technique adept at uncovering intricate patterns within high-dimensional data (LeCun et al., 2015), excels in simulating complex non-linear relationships in atmospheric systems (Liu et al., 2021), particularly for tasks involving multiple variables and objectives (Masmoudi et al., 2020; Huang et al., 2021). ML has been used to assist the modeling of RSM (Xing et al., 2020; Li et al., 2022), as well as the simulation of some key mechanisms to accelerate CTM simulation (Liu et al., 2021; Kelp et al., 2022). Recently, Huang et al. (2021) developed a neural network-based chemical transport model (NN-CTM) using advanced deep learning methods to independently approximate the actual CTM for simulating several air pollutants, showcasing the efficacy of machine learning in "emission-concentration" modeling without relying on RSM.

Transformer, as a renowned machine learning architecture characterized by the self-attention mechanism (Vaswani, 2017), has been substantially applied in the natural language process and image classification due to its ability of feature extraction and long-range dependency modeling (Devlin, 2018; Zhou et al., 2024). The self-attention mechanism facilitates the simultaneous evaluation of all positions within the input sequence and allows the model to discern dependencies across various species (Zhou et al., 2024), thus enabling the model to handle sophisticated high-dimensional data. The utilization of Transformer architecture for modeling in atmospheric science has become progressively more prevalent, exemplified by their incorporation into air quality forecasting, e.g. Informer (Zhou et al., 2021) and AirFormer (Liang et al., 2023), along with large-scale meteorological models for numerical weather prediction, such as Pangu (Bi et al., 2022), Fuxi (Chen et al., 2023c), and Fengwu (Chen et al., 2023b). This trend highlights the advantages of Transformer-based models over traditional approaches such as Random Forest and Multilayer Perceptron, especially in terms of their ability to capture complex patterns and relationships in data. However,

https://doi.org/10.5194/egusphere-2025-2186
Preprint. Discussion started: 28 May 2025

owing to the stringent requirements in terms of datasets (Narayanan et al., 2021) and hardware resources (Vaswani, 2017), the application of the Transformer architecture in "emission-concentration" predicting research has been limited.

In this study, we proposed an highly-efficient and informative air quality agent prediction model (TGEOS v1.0), which is based on Transformer architecture as a GEOS-Chem agent model. It is referred to as "TGEOS" throughout this paper. Relative to earlier studies, this research offers several significant benefits. First, TGEOS is able to predict the probability distribution of future air quality under different emission scenarios. Compared to solely average estimated by previous RSM methods, probability distribution can provide informative frequency distributions of pollutants (Yang and Wu, 2022). The probability distributions have been used to represent future states of $PM_{2.5}$ (Li et al., 2024) and O_3 (Zeng et al., 2022) concentrations in diverse emission scenarios, and to explore any extreme pollution events that are typically represented by the high-end tail of the probability distribution curve (Zhang et al., 2018; Lu et al., 2020a), as well as the related health impact (Tian et al., 2022).

Second, TGEOS is suitable for concentration prediction in more comprehensive scenarios that include multiple precursor emissions from multiple sectors. Specifically, in contrast to RSMs with scarce emission variables, sectoral emissions for 26 precursor emissions encompassing over 18 VOC species are incorporated into this model, which enhances the model's capacity to address more flexible demands of policymakers towards interested emission scenarios. Third, given the significant influence of regional transport on local pollutant concentrations (Qiao et al., 2021) and the inability of current technologies to simultaneously consider the impact of regional transport and detailed emission variables, the effects of adjacent grids consist of emission, meteorological conditions, as well as geo-spatial data are taken into account to ensure the accuracy of predictions. In addition, with the use of the Transformer framework, TGEOS demonstrates significantly enhanced predictive accuracy compared to established machine learning models like Multi-Layer Perceptron (MLP) and Random Forest (RF).

This paper is organized as follows: Section 2 introduces the dataset and methodology used for this study; Section 3 presents an in-depth analysis of TGEOS's performance on the test set, along with a comparative evaluation highlighting its advantages over alternative models; Conclusions are then summarized in Section 4.

2 Dataset and methodology

2.1 Dataset

To meet the demands of deep learning model training, we created a multi-scenario dataset based on several meticulously crafted emission scenarios and their corresponding GEOS-Chem simulations. The compilation of this dataset primarily consists of three components: generating multi-scenario emission inventories, conducting GEOS-Chem simulations, and assembling samples. The details of this process are discussed below.

2.1.1 Multi-scenario inventory

As a prerequisite to simulate future air quality, we first produced a multi-scenario emission inventory of 36 emission scenarios, including 24 future emission scenarios, 11 fine-tuned scenarios and 1 background scenario. Detailed information on the

https://doi.org/10.5194/egusphere-2025-2186
Preprint. Discussion started: 28 May 2025

inventory is shown in Table 1. We first used 24 future emission scenarios based on the DPEC (Dynamic Projection model for Emissions in China) platform (http://meicmodel.org.cn) to initially construct the data set. As a dynamic model developed by Tsinghua University (Tong et al., 2020), DPEC can reflect the dynamic changes of China's future emissions under various socioeconomic and policy control scenarios, and provide detailed gridded emission data, including emissions with different control scenarios, emission sectors and spatial coordinate information. Specifically, we designed two scenario sets of DPEC-SSP and DPEC-CA to represent emission scenarios under different socio-economic scenarios and different emission reduction policies, respectively. DPEC-SSP was selected from DPECv1.0 (Tong et al., 2020) and consists of five sub-scenario sets (SSP1-5). Data of 2030, 2040 and 2050 were selected in each sub-scenario, and each of them was treated as an independent emission scenario for our multi-scenario inventory. DPEC-CA was selected from DPECv1.2 (Cheng et al., 2023) and was composed of three sub-scenario sets including "clean air", "on-time peak-clean air", and "early peak-net zero-clean air". Similarly, we selected three years of data for each sub-scenario set as independent emission scenarios.

In addition, in order to improve the generalization ability of the model, we designed 10 random scenarios based on fine-tuning experiments, including emission scenarios with different emission factors ranging from 0 to 2.0 for each emission species and emission sector, so that the model can better understand the relationships between various features and model performance can be substantially improved. These emission factors were generated for representing the spatial variability that widely used in data assimilation (Jin et al., 2023). The detailed process for generating these stochastic emission factors is discussed in the Text S1.

For each emission scenario, we divided it by the 2017 MEIC inventory to obtain a series of monthly coefficient matrices for the emissions of various species in five sectors. It is worth noting that since the units of DEPC and MEIC data are tons per grid, significant variation are exhibited between adjacent grids. Thus, we set the maximum value of each coefficient matrix to 2.0 when making the DPEC scenarios to avoid abnormal emission coefficients due to magnitude differences. Subsequently, we multiplied the generated coefficient matrices to the corresponding part of the original inventory used for GEOS-Chem input to obtain the multi-scenario inventory that reflect the control of each scenario. The new inventory was employed in GEOS-Chem simulating to obtain $PM_{2.5}$ and O_3 concentrations under future emission scenarios.

2.1.2 GEOS-Chem configuration

The GEOS-Chem chemistry transport model (http://www.geos-chem.org, version 14.2.2) was used to simulate the spatiotemporal distribution of surface $PM_{2.5}$ and O_3 concentrations under different emission scenarios based on year 2017. The nested model was configured with a horizontal resolution 0.5° latitude by 0.625° longitude covering China (from 17.5 to 54°N and 72 to 136°E) and 47 vertical layers. Boundary condition files for model startup were offered by 1-year global GC simulation with a horizontal resolution of 2° latitude by 2.5° longitude. Assimilated meteorological data from the NASA Global Modeling and Assimilation Office's Modern-Era Retrospective analysis for Research and Applications Version 2 (MERRA-2) (Gelaro et al., 2017) were selected as meteorology fields entering the model. The Multi-resolution Emission Inventory for China (MEIC, http://meicmodel.org/) (Li et al., 2017) and the multi-scenario emission inventories with a horizontal resolution of 0.25° latitude by 0.25° (as detailed in 2.1.1) were used as the monthly anthropogenic emissions to simulate $PM_{2.5}$ and O_3 concentrations

https://doi.org/10.5194/egusphere-2025-2186
Preprint. Discussion started: 28 May 2025

Table 1. Description of multi-scenario inventory.

Scenario set	Sub-scenario set	Independent scenarios	Description
DPEC scenarios	DPEC-SSP	(1) SSP1 (2030, 2040, 2050)	SSP1-26-BHE control
		(2) SSP2 (2030, 2040, 2050)*	SSP2-45-ECP control
		(3) SSP3 (2030, 2040, 2050)*	SSP3-70-BAU control
		(4) SSP4 (2030, 2040, 2050)	SSP4-60-BAU control
		(5) SSP5 (2030, 2040, 2050)	SSP5-85-BHE control
	DPEC-CA	(1) ep (2030, 2040, 2050)	early_peak-net_zero-clean_air control
		(2) otp (2030, 2040, 2050)	on-time_peak-clean_air control
		(3) ca (2030, 2040, 2050)	clean_air control
Fine tuning scenarios	-	tun0.05, tun0.2, tun0.4, tun0.6, tun0.8, tun1.0, tun1.2, tun1.4, tun1.6, tun1.8, tun1.95	Random scenarios generated by tuning experiments
Background scenario	-	base2017	Original 2017 emission scenario

* Samples corresponding to six scenarios from SSP2 and SSP3 in the multi-scenario dataset were utilized for model testing, whereas the remaining samples were employed for model training.

under various emission scenarios. For anthropogenic emissions out of China, we used data from the Community Emissions Data System (CEDS) inventory (Hoesly et al., 2018).

2.1.3 Multi-scenario dataset

As demonstrated in Table 2, Sectoral emission data for 26 precursors across all grid cells in each scenario were utilized as training features. To account for pollutant transport from adjacent areas, emission data from the 8 grid cells surrounding the target grid were also incorporated as training features. Concurrently, 8 key meteorological parameters, previously demonstrated to exhibit significant correlations with $PM_{2.5}$ and O_3 concentrations (Shi et al., 2020; Zhang et al., 2022a), for both the target and neighboring grids derived from MERRA-2 data from 2017 were included as training features. Furthermore, local and peripheral spatial location information was incorporated as a training feature to enable the model to capture spatial patterns in pollutant emissions and concentrations. Finally, twelve statistical indicators, including the 25 quantile, 75 quantile, median, average, maximum, and minimum values that derived from the daily averaged concentrations of $PM_{2.5}$ and O_3 of a month, were utilized as training targets to represent the probability distribution of pollutant concentrations. It should be noted that this study mainly concentrates on the prediction of air quality in different scenarios of anthropogenic emissions, so the dust components were excluded during subsequent data processing.

https://doi.org/10.5194/egusphere-2025-2186
Preprint. Discussion started: 28 May 2025

Table 2. Targets and features for TGEOS model.

Target number	Training targets	Feature number	Training Features
12	Monthly average, maximum, minimum, median, 25 and 75 quantiles of $PM_{2.5}$ and O_3 concentrations	1045	(1) 5 sectors of 26 anthropogenic emissions with 8 adjacent emissions of each grid, e.g., NOx_industry, NOx_industry_adj1, and ALK3_residential_adj3. (2) 9 meteorological parameters with the 8 adjacent values of each grid, e.g., T2M, T2M_adj1, PBLH, PBLH_adj1. (3) local and adjacent longitude and latitude values, and month in each scenario.

2.2 Methodology

2.2.1 Model architecture

In previous "emissions-concentration" modeling, field-to-field modeling using the convolution neural networks (CNN) model has been widely used because of the efficient usage of the spatial relationship between features and concentrations (Xing et al., 2020; Huang et al., 2021). However, this approach may increase the demand for computational resources, especially when addressing considerable features. To address this issue, we built the TGEOS model based on a manageable sequence dataset (see Section 2.1) that integrated GC simulations for each grid cell, local and surrounding emissions, meteorological and spatial information. This approach models based on each grid while considering the impact of regional transport, thereby reducing the computational burden.

In this study, we employed an informative prediction model based on Transformer architecture comprising the encoder for feature extraction and the regressor for target mapping. In order to align with the shape of the dataset, the model was designed with 1048 input channels and 12 output channels. Six Encoder layers were configured with the model, each of which primarily incorporates a multi-head self-attention mechanism with eight attention heads and a feed-forward network. The multi-head self-attention mechanism was employed to capture the dependency relationships among various positions within the input sequence, while the feed-forward network facilitates additional nonlinear transformations on the features at each position (Vaswani, 2017). By leveraging the multi-head self-attention mechanism, the model can compute the similarity (or attention weights) of each feature in relation to all other features, thus producing a weighted representation for each position and determining the extent to which each position relies on information from others. Moreover, the feed-forward network, consisting of two fully connected layers, enhanced feature representation and improves the model's learning efficacy by incorporating nonlinear activation functions. In this implementation, the ReLU activation function was selected due to its ability to prevent negative values and expedite the model's training process (Nair and Hinton, 2010). Additionally, each sub-module incorporated residual connections and layer normalization to mitigate the risks of gradient disappearance or explosion. The output from the Encoder

https://doi.org/10.5194/egusphere-2025-2186
Preprint. Discussion started: 28 May 2025

undergoes global pooling to decrease model complexity. Finally, the regressor was comprised of fully connected layers that map the Encoder output to the specified output channels.

As depicted by Fig. 1, the model incorporates local and surrounding sectoral emissions for each grid, along with various meteorological parameters, to predict the probability distribution of pollutants under different scenarios, which is characterized by a series of concentration indicators including the average, maximum, minimum, median, 25 and 75 quantile of $PM_{2.5}$ and O_3. We selected six indicators for each pollutant as our prediction targets since the distributions of these two pollutants generally conform to either a standard normal or skewed distribution. The probability distribution curve would be quantified with these 6 indicators in the following test.

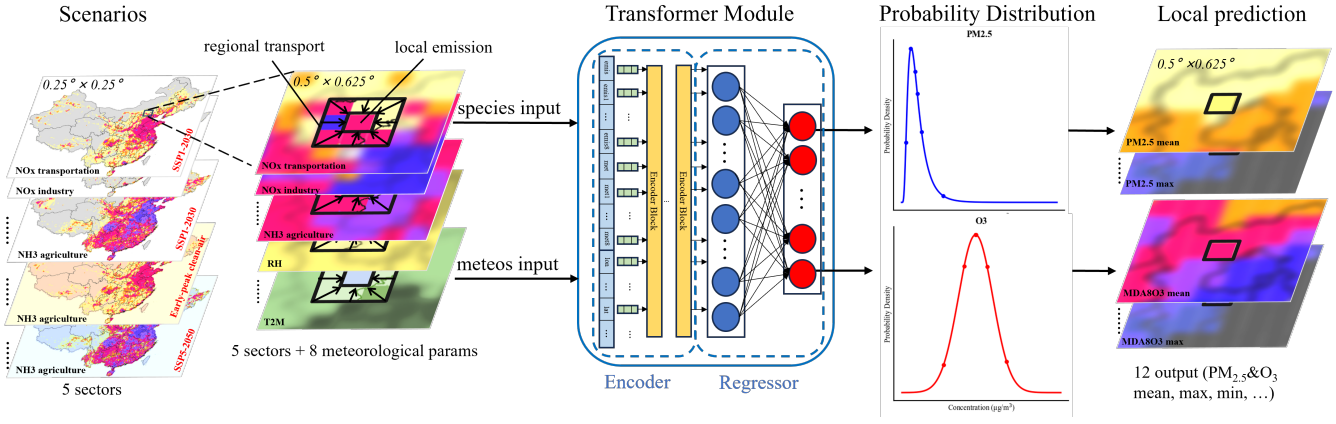

Figure 1. Flow scheme of TGEOS development.

2.2.2 Model training and evaluation

In this study, three machine learning models were employed independently to evaluate the performance for each kind of model structure. Except for the TGEOS model discussed in this paper, two conventional ML models, namely random forest (RF) and multi-layer perceptron (MLP), which had demonstrated good performance in air quality forecasting (Fang et al., 2023) were simultaneously employed based on the same training strategy.

The detailed dataset for model construction was derived from the multi-scenario inventory presented in Table 1. Samples from a total of 29 scenarios within the multi-scenario dataset were selected to construct the training set. While samples from six scenarios of SSP2 (SSP2_30, SSP2_40, SSP2_50) and SSP3 (SSP3_30, SSP3_40, SSP3_50) that representing low and high emission scenarios respectively were chosen to construct the test set.

In order to optimize the ability of TGEOS model to reproduce GEOS-Chem simulations, the mean squared error (MSE) was adopt as the loss function that measures the squared variance between TGEOS predicted (m_i) and GC simulated (g_i) concentrations to supervise the model training.

https://doi.org/10.5194/egusphere-2025-2186
Preprint. Discussion started: 28 May 2025

$$\mathcal{L}(m) = \frac{1}{N}\sum_{i=1}^{N}(m_i - g_i)^2 \quad (1)$$

The model weights were optimized with respect to the loss function using the Adam optimizer (Kingma, 2014) with an learning rate is 1×10^{-4}. To save the optimal model weights during training, 20% of the randomly sampled training data were set aside for model validation purposes. The model was trained for 100 epochs with a batch size of 64. To reduce the risk of overfitting, we applied L2 weight regularization on all trainable parameters during training and fine-tuning.

The performance of TGEOS was evaluated using two statistical indices, namely, R-Square (R^2) and Mean Absolute Error (MAE), which are commonly used in evaluating the performance of CTM emulating (Salman et al., 2024). Their corresponding mathematical formulas are delineated as follows.

$$R^2 = 1 - \frac{\sum_{i=1}^{N}(m_i - g_i)^2}{\sum_{i=1}^{N}(m_i - \bar{m})^2} \quad (2)$$

$$MAE = \frac{1}{N}\sum_{i=1}^{N}|m_i - g_i| \quad (3)$$

Here m_i and g_i denote the TGEOS-predicted and GC-simulated pollutant concentrations, respectively. Indices i means the ith grid cell. $\bar{m}$ is the average of all the model-predicted samples and N refers to the number of samples from the training set.

3 Results and discussions

The overall performance of TGEOS on the test set is shown in Table S1. We found that the model performed well across all target indicators. The R^2 ranges from 0.958 to 0.992, with relatively low RMSE and MAE, averaging 2.808 $\mu g/m^3$ and 1.588 $\mu g/m^3$, respectively. The following presents detailed analyses: Section 3.1 focuses on analyzing the differences between the training set and the test set; Section 3.2 and 3.3 involves predicting spatial and probability distributions of $PM_{2.5}$ and O_3 concentrations; Section 3.4 is dedicated to comparison of different models.

3.1 Differences between training and test set

In case of potential data leakage due to similar concentration and emission levels in some emission scenarios, we analyzed the spatial distribution of the mean values of $PM_{2.5}$ and O_3 under the stochastically selected SSP_2050 scenario of the test set, along with the otp2030 scenario of the training set that exhibiting the highest similarity in concentration levels of SSP_2050 scenario. Focusing on the North China Plain (NCP) region where both $PM_{2.5}$ and O_3 pollution are severe, the absolute difference in concentration between two scenarios was demonstrated. Concurrently, distributions of six emission variables of two scenarios with significant impacts on $PM_{2.5}$ and O_3 concentrations (Hu et al., 2023), as well as the differences, were also

https://doi.org/10.5194/egusphere-2025-2186
Preprint. Discussion started: 28 May 2025

analyzed. The spatial distribution of the concentration, emission, and absolute difference levels of $PM_{2.5}$ are shown in Fig. 2, and those of O_3 are illustrated in Fig. S1. These pictures indicated that the concentrations of pollutants, as well as emission variables, of the training and test set are exclusive despite some distributional similarities, particularly for samples from highly polluted regions.

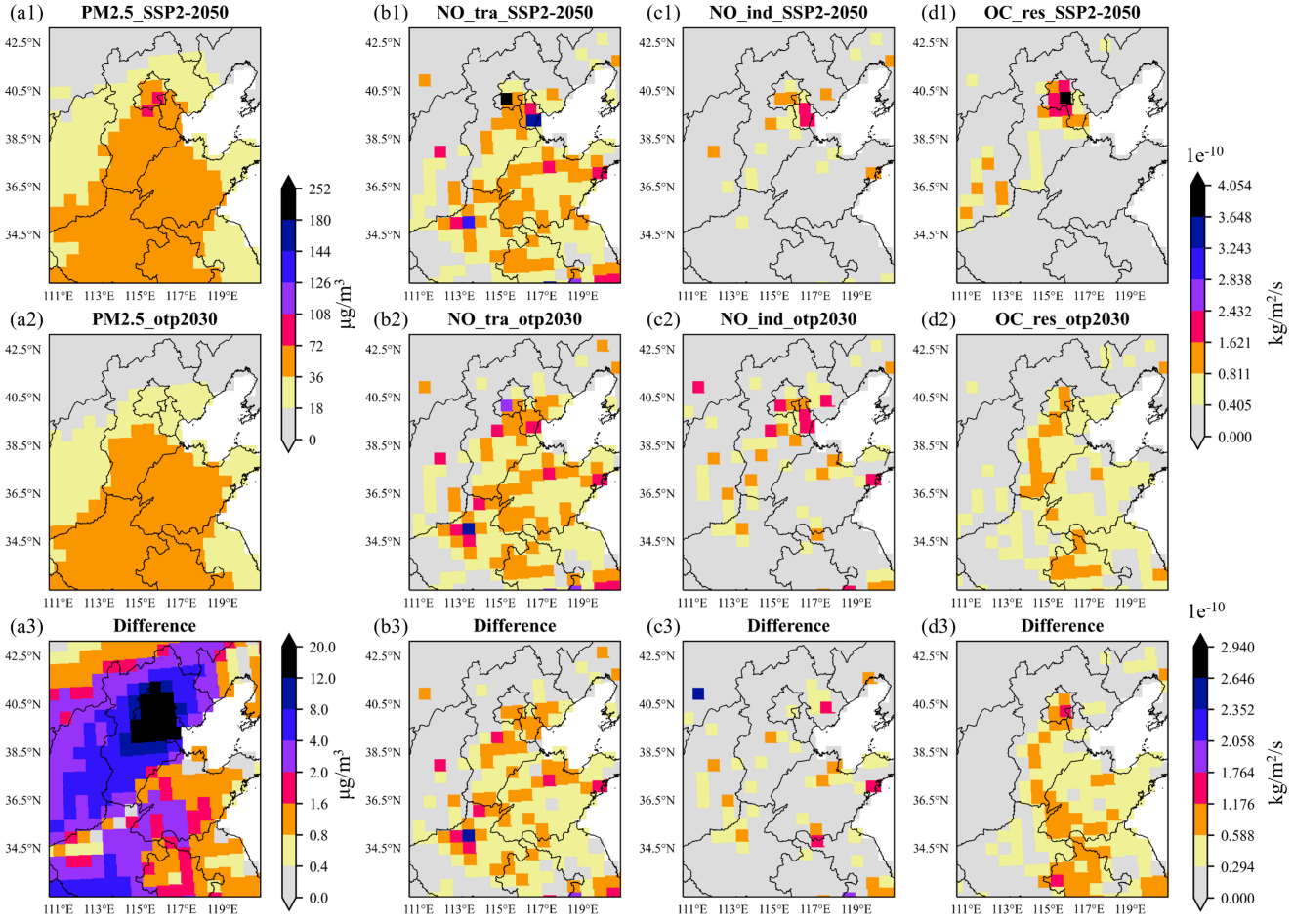

Figure 2. Spatial distributions of mean $PM_{2.5}$ concentration and three emission variables in SSP2_2050 (a) and otp2030 (b) scenarios in January, along with the quantified absolute differences between two scenarios (c).

3.2 Prediction of spatial distribution of $PM_{2.5}$ and O_3

We first evaluated the spatial distribution performance of TGEOS predictions of $PM_{2.5}$ and O_3 for 6 test scenarios. For the sake of brevity, we presented the results of two test scenarios, namely SSP2_2040 and SSP3_2040, to represent the low and high emission scenarios. Additionally, we focused on the months with the highest concentrations of $PM_{2.5}$ and O_3 to better visualize

https://doi.org/10.5194/egusphere-2025-2186
Preprint. Discussion started: 28 May 2025

the spatial distribution of pollutants. Figure 3 and S2 present the spatial comparison of $PM_{2.5}$ concentration indicators between GC and TGEOS for SSP2_40 and SSP3_40 scenario in January.

The results demonstrate that, across various emission scenarios, the spatial distribution of $PM_{2.5}$ concentrations simulated by TGEOS exhibits a high degree of similarity with that produced by GC. Specifically, TGEOS effectively captures the spatial distribution patterns of $PM_{2.5}$ concentrations, accurately identifying high-pollution zones in central and northern China, alongside low-pollution areas in other regions. Furthermore, the disparities observed in $PM_{2.5}$ concentration levels under distinct emission scenarios indicate that TGEOS has successfully discerned the intricate relationships between precursor emissions and $PM_{2.5}$ concentrations. Beyond its capability to predict monthly mean values, TGEOS also excels in predicting additional statistical indicators associated with $PM_{2.5}$ concentrations, including the maximum concentrations of significant concern to policymakers as well as the 25th and 75th quantile, which reflect the distribution of concentrations. Other statistical indicators, such as the median and minimum values that shown in Fig. S4, are also effectively predicted.

As illustrated in Fig. 5(a), S6(a), and S7(a), there exists a robust statistical correlation between the $PM_{2.5}$ indicators predicted by TGEOS and the actual GC simulations across varying emission scenarios, with R^2 values ranging from 0.976 to 0.995. These results substantiate that $PM_{2.5}$ accurately captures the principal trends and patterns of $PM_{2.5}$ as simulated by GC. Moreover, the evaluation of model prediction errors, as quantified by the Root Mean Square Error (RMSE) and Mean Absolute Error (MAE), reveals relatively low error levels, with RMSE values ranging from 0.985 to 2.110 and MAE values between 0.685 and 3.243. This underscores the reliability of TGEOS predictions in relation to those achieved by the GC simulations. In other words, the predictive capabilities of TGEOS are characterized by a high degree of accuracy and reliability.

The spatial comparison of O_3 concentration indicators between GC and TGEOS for two scenarios in July are presented in Fig. 4, S3, and S5. Similar to the predictions for $PM_{2.5}$, we observed that TGEOS successfully captures the spatial distribution patterns of O_3 as simulated by GC, as well as the concentration differences resulting from various emissions. The scatter density plots presented in Fig. 5(b), S6(b), and S7(b) indicate a strong correlation between TGEOS and GC, with R^2 values ranging from 0.966 to 0.996. Additionally, the accuracy of TGEOS predictions is further supported by the relatively low RMSE values, which range from 0.985 to 2.110, and MAE values ranging from 1.593 to 4.933. These results demonstrate that TGEOS is capable of accurately and reliably predicting both $PM_{2.5}$ and O_3 concentration distribution across different scenarios, achieving a level of performance comparable to that of GC.

The error graphs of $PM_{2.5}$ indicators for SSP2_40 and SSP3_40 are shown in Fig. 3 a3 to d3 and Fig. S2 a3 to d3. We found the model exhibits relatively large errors in predicting the monthly maximum concentrations of $PM_{2.5}$. This is attributed to the inherent randomness of these peak values compared to other indicators, which poses challenges for accurate prediction. Furthermore, our analysis indicates the presence of both overestimation and underestimation within these error graphs. On one hand, the GC simulations for each scenario in this study are driven by a fixed initial concentration file derived from a background scenario, with monthly concentration predictions treated as independent and not accounting for the influence of the initial concentration field. This approach may introduce discrepancies between the model predictions and the actual GC simulations, particularly when the pollutant concentration levels deviate significantly from those in the initial concentration file. This phenomenon elucidates why the predictive performance under the SSP2 scenario, as illustrated in Fig. 5 and S6, is

https://doi.org/10.5194/egusphere-2025-2186
Preprint. Discussion started: 28 May 2025

somewhat inferior to that observed under the SSP3 scenario, as well as the patterns of overestimation and underestimation evident in the error maps for each scenario.

The predictions from TGEOS also demonstrate a clear pattern of seasonal variation. Here, we focus on two statistical indicators that are crucial for fitting the probability distribution curve, namely the 25th quantile and the 75th quantile, and select results from January, April, July, and October to represent the distribution of pollutants during winter, spring, summer, and autumn, respectively. Figure 6 and 7 illustrate the seasonal variation of $PM_{2.5}$ and O_3 indices predicted by TGEOS under two emission scenarios. The R^2 values for the 25th and 75th quantile of $PM_{2.5}$ are 0.964 to 0.994 and 0.973 to 0.996, respectively, while those for O_3 are 0.903 to 0.994 and 0.946 to 0.994, respectively, indicating a strong correlation between predicted and simulated pollutant concentrations across all seasons.

Specifically, TGEOS effectively captures the seasonal trends and patterns of $PM_{2.5}$ and O_3 as simulated by GEOS-Chem. Seasonal variations in both pollutants are evident, with $PM_{2.5}$ concentrations gradually decreasing from winter to summer (Fig. 6 a1 to a3 and Fig. 6 b1 to b3), while ozone concentrations exhibit a gradual increase during the same period (Fig. 7 c1 to c3 and Fig. 7 d1 to d3). Furthermore, the accuracy of TGEOS predictions is noteworthy, as evidenced by the low MAE values for the 25th and 75th quantiles of $PM_{2.5}$ (0.297 to 0.832 and 0.670 to 1.561, respectively) and O_3 (1.186 to 2.952 and 1.186 to 3.631), indicating that TGEOS predictions closely align with GC simulations, despite some acceptable margin of error. Although the performance during periods of low concentration was less optimal, TGEOS demonstrated decent effectiveness during critical months when elevated concentrations and extreme pollution events are more likely to occur, particularly for $PM_{2.5}$ in January and O_3 in July.

From the perspective of predicting the spatial distribution of pollutants, although some discrepancies exist, TGEOS exhibits relatively high accuracy and reliability in predicting $PM_{2.5}$ and O_3 concentrations during key pollution months and across various seasonal pollution conditions compared to the corresponding simulations from GC.

3.3 Prediction of probability distribution of $PM_{2.5}$ and O_3

The probability distribution offers a comprehensive representation of pollutant concentrations over a specified time period and effectively captures extreme values, which are typically reflected in the tails of the probability distribution curve. Leveraging this advantage, probability distributions are critical in various air pollution studies, including investigations into future air quality under different emission scenarios (Zeng et al., 2022) or climate changes (Li et al., 2024), and potential mortality in heavily polluted regions (Tian et al., 2022). In this study, we focus on the probability distributions predicted by TGEOS for four key polluted areas: the North China Plain (NCP), Yangtze River Delta (YRD), Fenwei Plain (FWP), and Sichuan Basin (SCB). For each region, we calculated the average of twelve statistical indicators across all grid points and subsequently utilized these averaged indicators to fit the probability distribution curves for $PM_{2.5}$ and O_3.

The $PM_{2.5}$ concentration distributions from GC simulations and TGEOS predictions for the North China Plain (NCP), Yangtze River Delta (YRD), Fenwei Plain (FWP), and Sichuan Basin (SCB) in SSP2_2040 and SSP3_2040 are illustrated in Fig. 8. Additional results, encompassing four scenarios for the years 2030 and 2050, are presented in Fig. S8 and S10. We found the probability distribution curves of $PM_{2.5}$ concentration that TGEOS predicted in these regions exhibit a strong

https://doi.org/10.5194/egusphere-2025-2186
Preprint. Discussion started: 28 May 2025

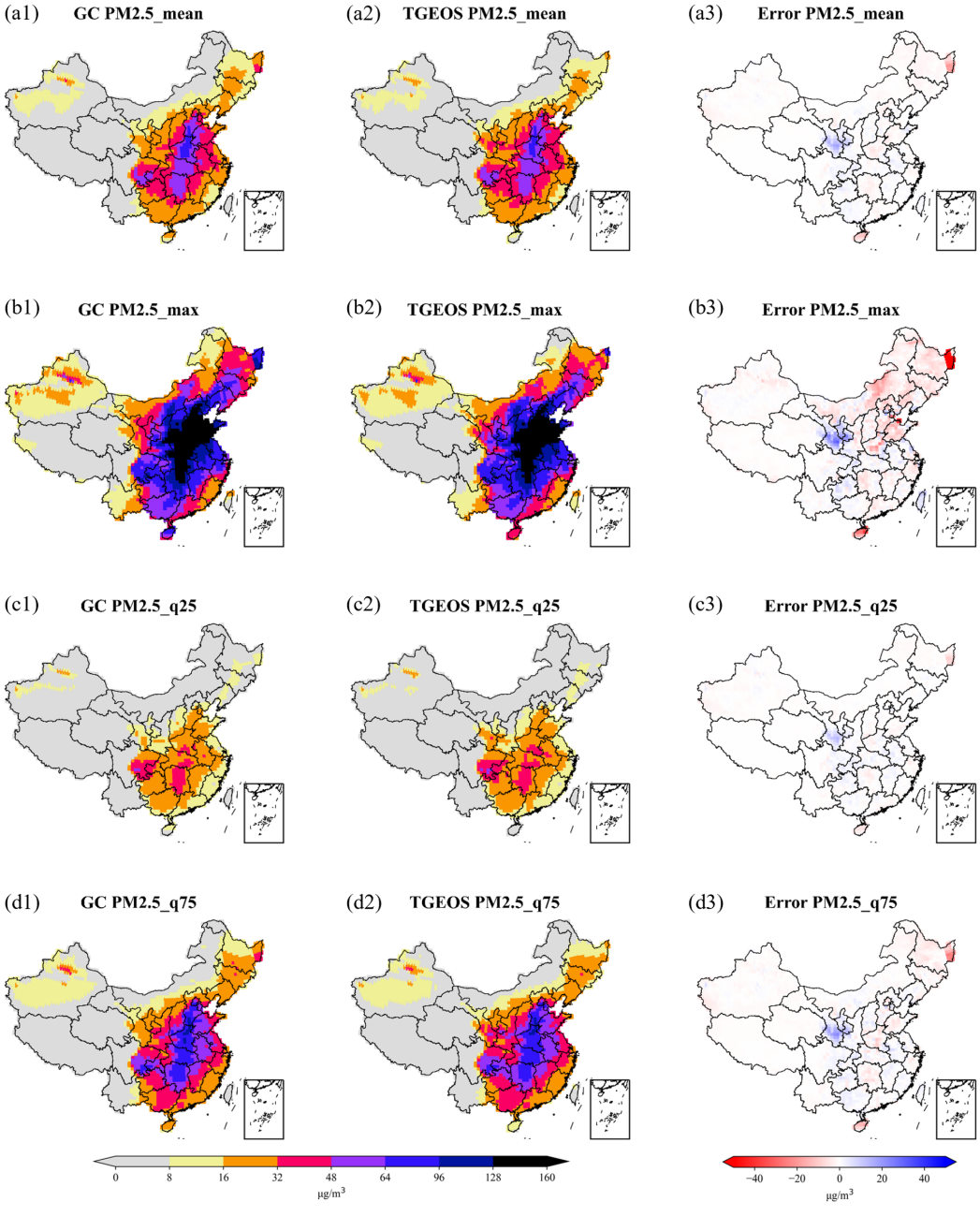

Figure 3. Spatial comparison of GEOS-Chem simulated and TGEOS estimated four statistical indicators of $PM_{2.5}$ concentrations in January under SSP2_2040 scenario (low emissions) and the corresponding error maps. (a1) to (d1) represent GC simulation while (a2) to (d2) represent TGEOS prediction, and (a3) to (d3) represent the error between this two for each indicator, including mean, maximum, 25-quantile, and 75-quantile.

https://doi.org/10.5194/egusphere-2025-2186
Preprint. Discussion started: 28 May 2025

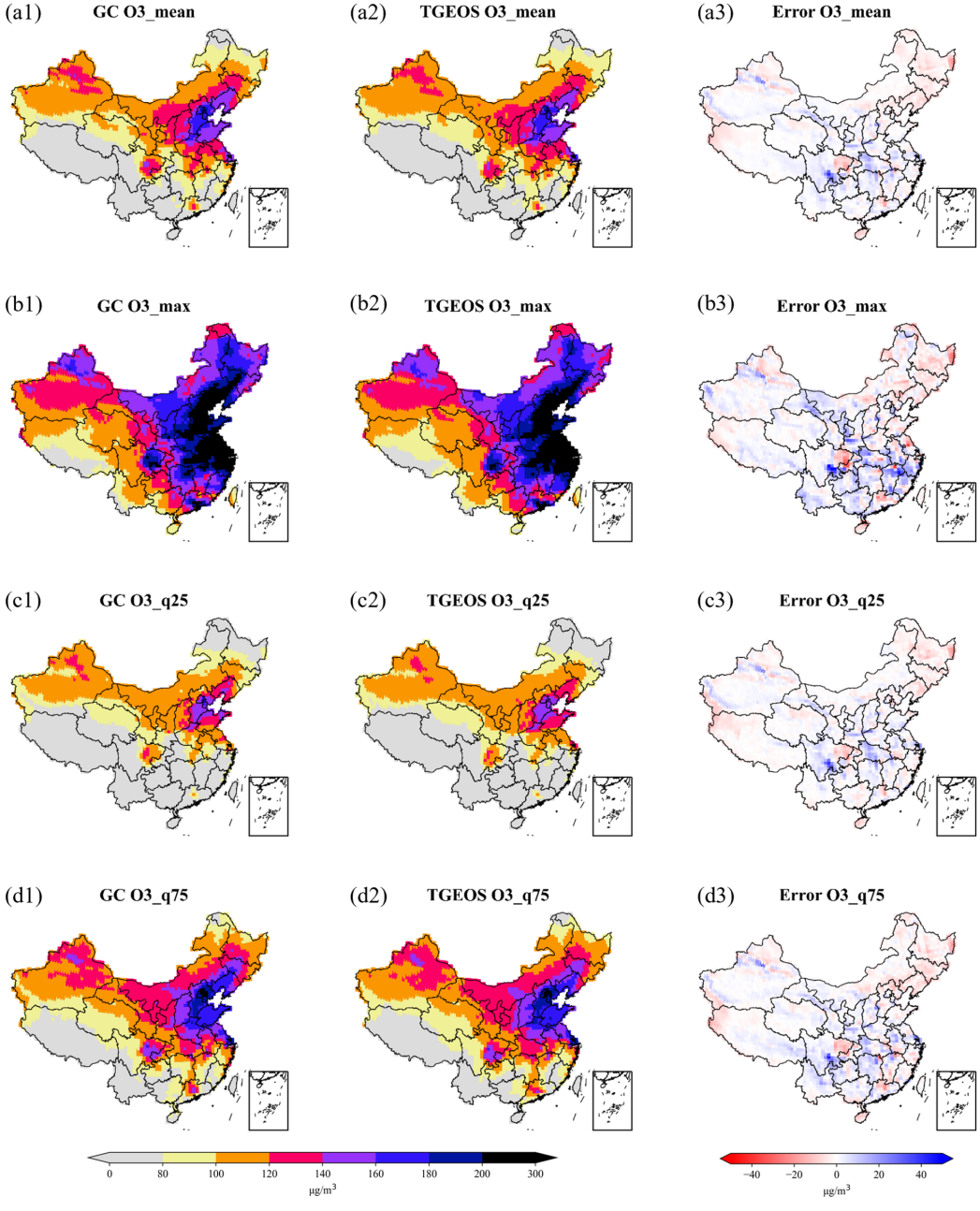

Figure 4. Spatial comparison of GEOS-Chem simulated and TGEOS estimated four statistical indicators of O_3 concentrations in July under SSP2_2040 scenario (low emissions) and the corresponding error maps. (a1) to (d1) represent GC simulation while (a2) to (d2) represent TGEOS prediction, and (a3) to (d3) represent the error between this two for each indicator, including mean, maximum, 25-quantile, and 75-quantile.

https://doi.org/10.5194/egusphere-2025-2186
Preprint. Discussion started: 28 May 2025

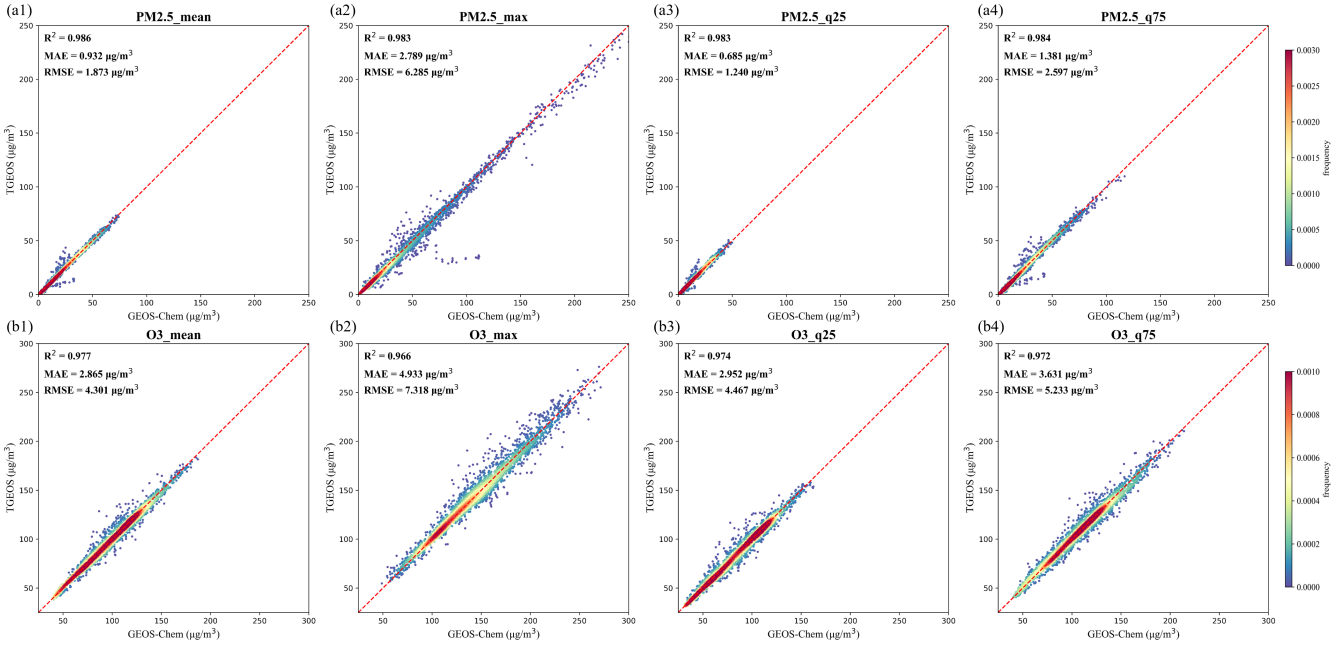

Figure 5. Density scatter plots between GEOS-Chem simulations and TGEOS predictions for eight indicators of $PM_{2.5}$ (a) and O_3 (b) concentrations in SSP2_2040 scenario. (a1 to a4) denotes the mean, maximum, 25th quantile, and 75th quantile of January $PM_{2.5}$ concentration; (b1 to b4) denotes the corresponding statistics for July O_3 concentration.

correlation with corresponding GC curves, indicating that TGEOS model has successfully established the relationship between $PM_{2.5}$ concentration and emissions of precursors in different regions for varying scenarios.

The effects of different emission scenarios are clearly reflected. We found that in low-emission scenarios (a1 to d1), the $PM_{2.5}$ probability curves for all four regions exhibited significant changes. The reduction in precursor emissions led to a decrease in overall $PM_{2.5}$ concentrations, resulting in an increase in lower values. This caused the peak of the curve to shift to the left relative to the base curve and become sharper. In contrast, in high-emission scenarios (a2 to d2), the increase in precursor emissions resulted in higher $PM_{2.5}$ concentrations, shifting the peak to the right and displaying a trend towards flattening.

Figure 9, S9, and S11 illustrate the O_3 concentration distributions predicted by TGEOS for NCP, SCB, YRD, and FWP. Similar to $PM_{2.5}$, the probability distribution curves of O_3 predictions show good agreement with GC curves. TGEOS also established the relationship between ozone concentrations and emissions in these regions, and successfully predicted the probability distribution of concentrations under various test scenarios. In high emission scenarios, excessive precursor emissions elevate overall O_3 pollution levels, resulting in the occurrence of more high-value concentrations. This flattens the distribution curve of O_3 compared to the base curve, while also lowering its peak value. Conversely, in low emission scenarios, the reduction of precursor pollutants—such as nitrogen oxides (NO_x) and volatile organic compounds (VOC_s), which significantly

https://doi.org/10.5194/egusphere-2025-2186
Preprint. Discussion started: 28 May 2025

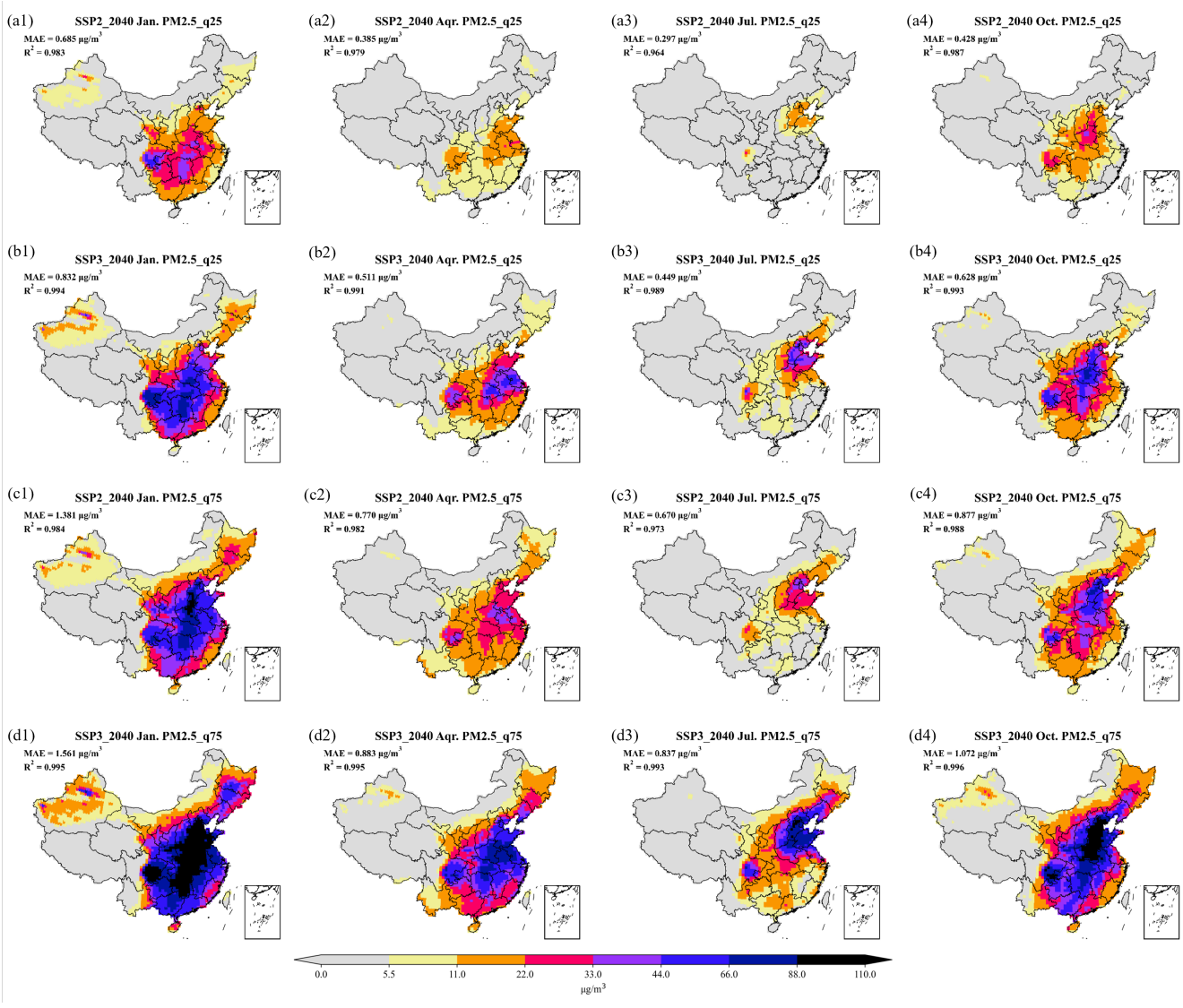

Figure 6. Spatial distribution of 25th and 75th quantile of $PM_{2.5}$ concentrations estimated by TGEOS in January, April, July and October under SSP2_2040 and SSP3_2040 scenarios. (a) and (b) illustrate the TGEOS estimates for the 25th quantile of $PM_{2.5}$ under the SSP2_2040 and SSP3_2040 scenarios from January to October. Conversely, (c) and (d) depict the TGEOS estimates for the 75th quantile of $PM_{2.5}$ under the same scenarios during the same months.

https://doi.org/10.5194/egusphere-2025-2186
Preprint. Discussion started: 28 May 2025

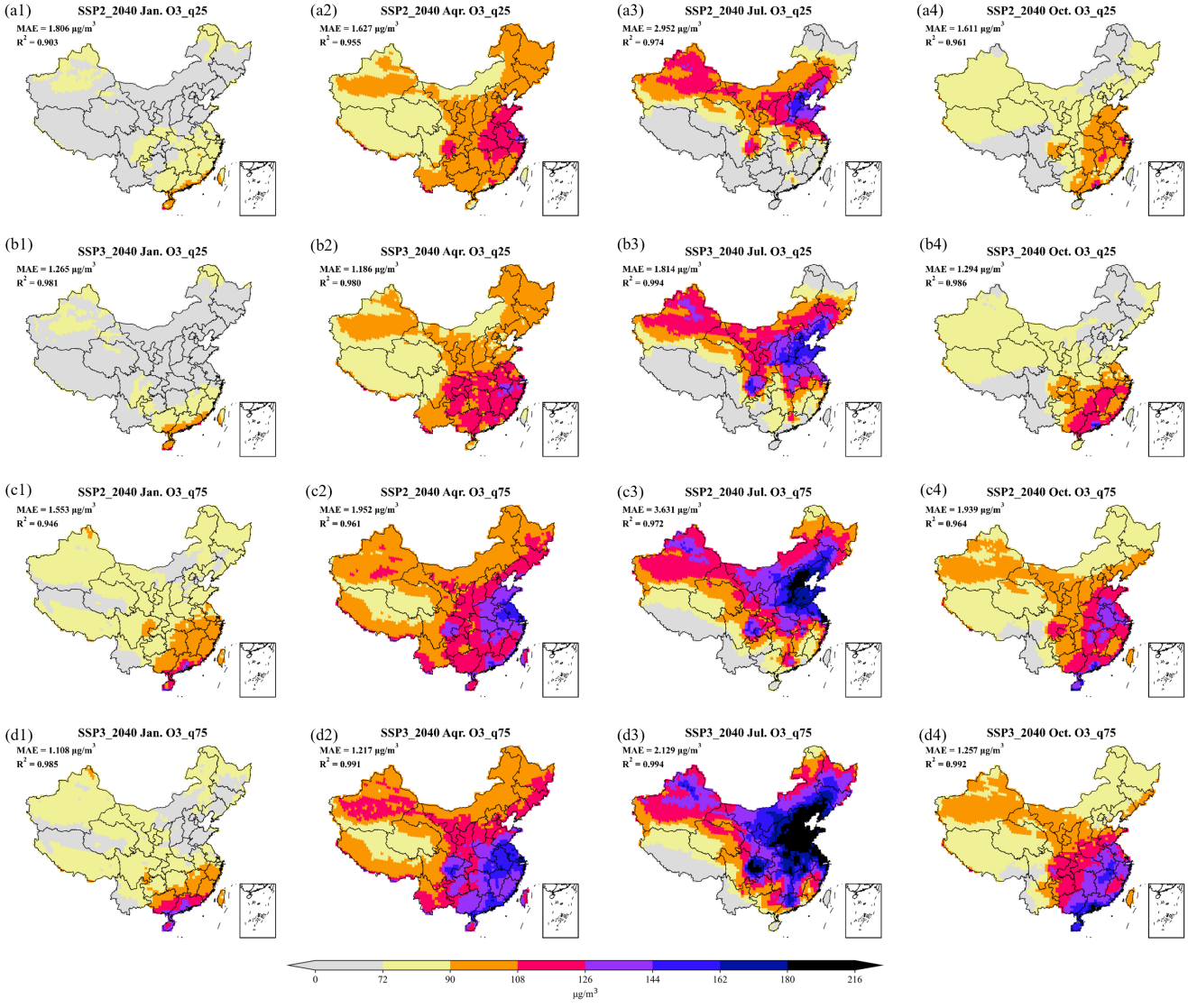

Figure 7. Spatial distribution of 25th and 75th quantile of O_3 concentrations estimated by TGEOS in January, April, July and October under SSP2_2040 and SSP3_2040 scenarios. (a) and (b) illustrate the TGEOS estimates for the 25th quantile of O_3 under the SSP2_2040 and SSP3_2040 scenarios from January to October. Conversely, (c) and (d) depict the TGEOS estimates for the 75th quantile of $PM_{2.5}$ under the same scenarios during the same months.

https://doi.org/10.5194/egusphere-2025-2186
Preprint. Discussion started: 28 May 2025

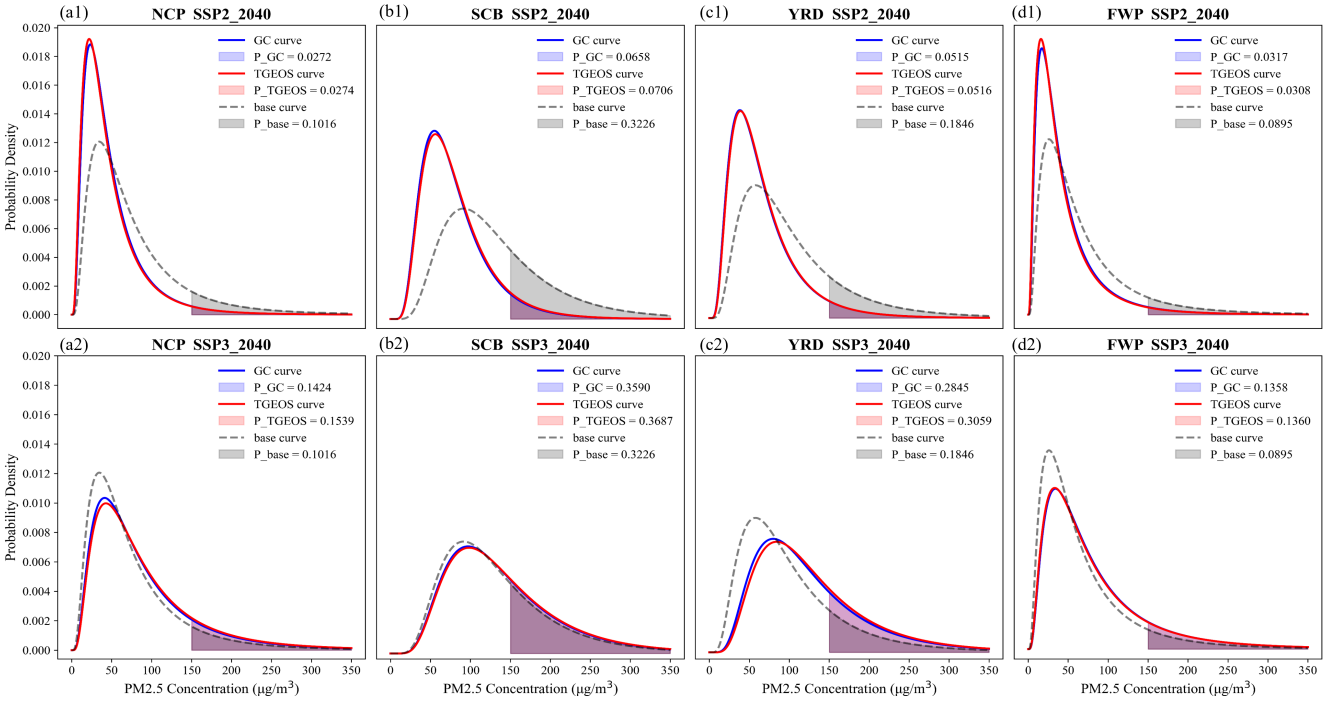

Figure 8. Probability distribution curves of winter $PM_{2.5}$ fitted by GC and TGEOS estimates under two scenarios (SSP2_2040 and SSP3_2040) in four interest regions, including NCP (a), SCB (b), YRD (c), and FWP (d). The blue solid line and the red solid line represent the probability distribution curve of GC and TGEOS results. The black dashed line shows the distribution of pollutants in 2017 (background scenario). P_GC, P_TGEOS and P_base represent the probability of extreme pollution events (calculated from colored areas of each curve) in GC simulation, TGEOS prediction, and 2017 simulation.

influence ozone formation—leads to a decrease in O_3 concentration. This also sharpens the O_3 distribution curve and enhances its peak value. Compared to the notable variations observed in $PM_{2.5}$ levels, O_3 concentrations are relatively less influenced by emissions. This is largely due to the fact that ozone levels are predominantly determined by meteorological conditions, particularly air temperature, while all scenarios in this study are modeled using meteorological data from 2017, significant fluctuations are not expected.

Additionally, we observed that the model performs slightly poorly in predicting the probability distribution of pollutants under certain high emission scenarios (a2 to d2). As discussed in section 3.3, this discrepancy arises from the limited number of high-emission samples in the dataset, which undermines the model's generalization capabilities. It is also important to emphasize that when predicting O_3 levels under the SSP2_2050 scenario, the model demonstrates a systemic underestimation, as shown in Fig. S11 (a1 to d1). A detailed analysis of the emission data for this scenario indicates that several key precursors for O_3 generation, including ALK4, ALK5, and TOLU, exhibit relatively high emission levels in the SSP2_2050 scenario.

https://doi.org/10.5194/egusphere-2025-2186
Preprint. Discussion started: 28 May 2025

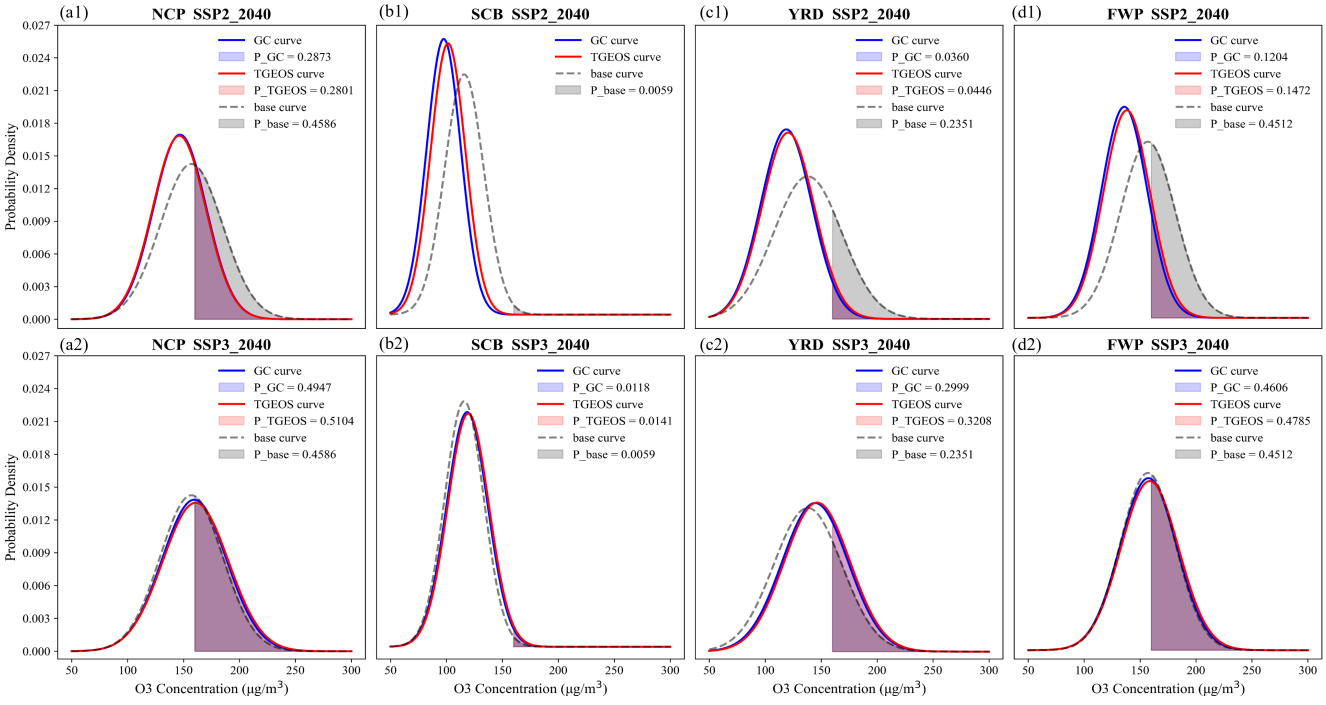

Figure 9. Probability distribution curves of summer O_3 fitted by GC and TGEOS estimates under two scenarios (SSP2_2040 and SSP3_2040) in four interest regions, including NCP (a), SCB (b), YRD (c), and FWP (d). The blue solid line and the red solid line represent the probability distribution curve of GC and TGEOS results. The black dashed line shows the distribution of pollutants in 2017 (background scenario). P_GC, P_TGEOS and P_base represent the probability of extreme pollution events (calculated from colored areas of each curve) in GC simulation, TGEOS prediction, and 2017 simulation.

The scarcity of high-emission samples for these species prevents the model from adequately recognizing the importance of high-emission features to the target variable, leading to a tendency for the model to underestimate predictions.

Furthermore, we utilized TGEOS to predict the probability of extreme pollution events under various emission scenarios. According to the China National Ambient Air Quality Standard (GB3095-2012), we set 150 μg/m^3 and 160 μg/m^3 for $PM_{2.5}$ and O_3 concentrations as thresholds of extreme pollution events, and then calculated the probability of exceeding these thresholds by integrating the fitted probability density functions to the right, represented by the shaded areas shown in the previous images. In the graphs depicting extreme events, the probability of extreme events calculated using the TGEOS curve (represented by the red shaded area) closely matches the probability calculated using the GC curve (represented by the blue shaded area). This concordance demonstrates that TGEOS has effectively learned the distribution patterns of high-concentration pollutants and its capability to predict potential extreme pollution events under future emission scenarios.

Our findings indicate that under low-emission scenarios, the incidence of extreme $PM_{2.5}$ events decreased most significantly in the SCB and YRD regions, as illustrated in (b1) and (c1). Compared to the base scenario, the incidence in the SCB region

https://doi.org/10.5194/egusphere-2025-2186
Preprint. Discussion started: 28 May 2025

decreased by 23.0%, 25.2%, and 27.4%, while in the YRD region, it decreased by 18.1%, 19.6%, and 20.6%, respectively. This indicates that implementing precursor emission reductions in these two regions can effectively control the occurrence of extreme $PM_{2.5}$ events. In contrast, under high-emission scenarios, the increase in incidence for each region was relatively small, approximately 4% to 5%. For extreme ozone events, the reduction effects were most pronounced in the NCP and FWP regions. As presented in (a1) and (d1), under the three low-emission scenario SSP2 scenarios, the incidence of extreme O_3 events in the NCP region decreased by 17.7%, 19.9% and 22.8%, while in the FWP region, it decreased by 18.6%, 23.4% and 27.7%, respectively. Furthermore, as shown in (c1), the YRD region experienced a reduction of approximately 18%. This demonstrates that precursor emission reductions in areas with high O_3 pollution are highly effective. Conversely, when emission levels increase, the risk of extreme O_3 events in these high-pollution regions rises sharply. Under the three high-emission scenario SSP3 conditions, the risk of extreme O_3 events in the YRD region increased by 12.8%, 13.3% and 14.9%, while in the FWP region, it increased by 8.2%, 9.7% and 10.6%. The changes in the NCP region were less noticeable.

The results above illustrate the impact of different emission scenarios on pollutant concentrations. Under consistent meteorological conditions, significant changes in the concentration distribution of both pollutants can be achieved through straightforward emission reductions, which notably mitigates extreme pollution risks in several heavily polluted areas. Therefore, it is essential to develop strategies to address the current state of air pollution. Furthermore, the TGEOS model shows a high level of similarity to the GC model in predicting pollutant distribution and extreme events, making it a valuable tool for online assessments of related emission reduction policies to enhance decision-making efficiency.

3.4 Comparison of different machine learning models

To validate the performance of the TGEOS model in "emission-concentration" modeling against other machine learning models, two widely used machine learning models, including multilayer perceptrons (MLP) and random forests (RF), were simultaneously employed based on the multi-scenario dataset mentioned in Section 2.1. For each ML model, we identified the model that demonstrated optimal fitting performance for testing after conducting a series of parameter tuning experiments. The MLP model uses 4 hidden layers with 2048, 1024, 512, and 256 neurons, applying ReLU activation and Dropout to prevent overfitting. The optimizer is Adam with a learning rate of $1e^{-3}$, and the loss function is Mean Squared Error (MSE). Training uses a batch size of 1024 and 100 epochs, with a learning rate scheduler to adjust the learning rate dynamically. The RF model uses 300 trees with a maximum depth of 25, a minimum sample split of 4, and a minimum sample per leaf of 2. It uses parallel computation with all CPU cores and performs feature selection by choosing the top 500 important features.

Table S2 and S3 summarize the performance of the three models on the test set. We found that TGEOS outperforms the other two models in both R^2 and MAE metrics. To clearly illustrate the predictive performance of different models, we presented a modified Taylor diagram (Taylor, 2005; Fang et al., 2023) in Fig. 10. This diagram simultaneously displays the Mean Absolute Error (MAE) and correlation coefficient (R) for predictions of $PM_{2.5}$ and O_3 indicators from three models in various regions. Our findings indicate that the Random Forest (RF) model performs the poorest. This is primarily due to its reliance on feature importance assessments during feature selection, which overlooks potential underlying features in the data, adversely affecting the model's fitting capability. Additionally, the RF model is sensitive to the distribution of training data, leading to limited

https://doi.org/10.5194/egusphere-2025-2186
Preprint. Discussion started: 28 May 2025

extrapolation abilities and poor predictive performance for extreme values. In contrast, the Multi-Layer Perceptron (MLP) shows a significant improvement in predictive performance relative to the RF model. Leveraging its multi-layer neural network structure, the MLP can more effectively learn complex relationships between multiple features. But this layered structure can struggle when dealing with high-dimensional feature spaces, especially for highly stochastic indicators such as maximum values, where the MLP still exhibits considerable prediction errors.

Conversely, the Transformer-based TGEOS model demonstrates superior performance compared to the other models, exhibiting higher R values (exceeding 0.98 and 0.97) and lower MAE values (less than 4.0 $\mu g/m^3$ for the majority indicators). These results suggest a higher degree of reliability and accuracy in its predictions. For several indicators where MLP performs poorly, TGEOS demonstrates substantial improvements. The superiority of the Transformer model can be attributed to its greater number of parameters and more complex architecture, which leverage powerful feature extraction capabilities and self-attention mechanisms, allowing it to adapt to intricate patterns and relationships. Consequently, in high-dimensional tasks like air quality modeling, Transformer models have proven to be more advantageous compared to their counterparts.

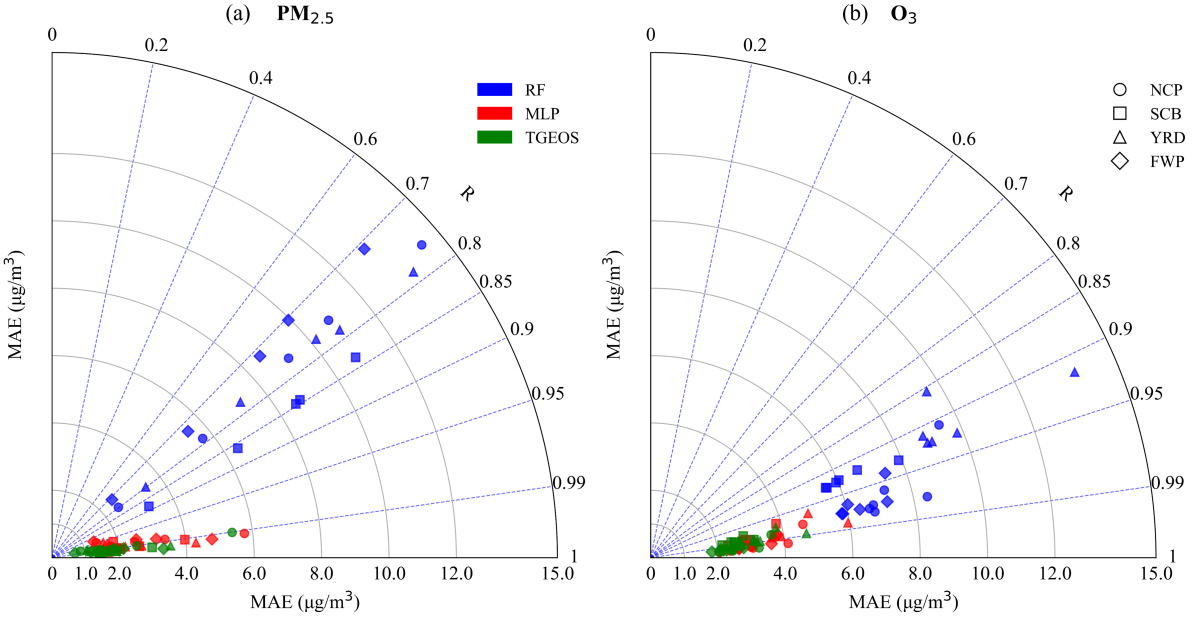

Figure 10. A modified Taylor diagram is presented to jointly illustrate the Mean Absolute Error (MAE) and correlation coefficient (R). The regions of interest, namely NCP, SCB, YRD, and FWP, are distinguished using unique markers: circle for NCP, square for SCB, triangle-up for YRD, and diamond for FWP. Furthermore, the concentration indicators of $PM_{2.5}$ and O_3 predicted from different models are visualized using distinct colors, where blue represents RF predictions, red denotes MLP predictions, and green indicates TGEOS predictions. All indicators are computed based on the six test scenarios.

https://doi.org/10.5194/egusphere-2025-2186
Preprint. Discussion started: 28 May 2025

4 Conclusions

In this study, we developed a Transformer-based information prediction model "TGEOS v1.0" that serve as a GEOS-Chem proxy model to represent future air quality under different emission scenarios. Based on GEOS-Chem version 14.2.2, TGEOS has successfully established the complex relationship between precursor emissions and concentrations of $PM_{2.5}$ and O_3 pollutants, which can be used for rapid online assessment of the effects of different emission control schemes. With exceptional computational efficiency, TGEOS can perform one-year predictions in about 2.51 seconds. Compared to previous studies that focus solely on average predication, TGEOS can predict the probability distribution of $PM_{2.5}$ and O_3 concentrations in different regions. Leveraging the strengths of high-dimensional data modeling inherent in the Transformer model, TGEOS is capable to provide more accurate predictions based on more detailed emission scenarios that take into account multiple precursor species, emission sectors, and adjacent emissions.

The air quality prediction of TGEOS for future emission scenarios has good correlation and accuracy with the actual output of GEOS-Chem. The R^2 ranges from 0.958 to 0.992, and the RMSE and MAE are relatively low, with mean values of 2.808 and 1.588 $\mu g/m^3$, respectively. TGEOS effectively predicted the spatial distribution of $PM_{2.5}$ and ozone concentration indicators across various emission scenarios, capturing their seasonal variations, and exhibiting an overall spatial distribution pattern that aligns well with the corresponding GC simulations. For another thing, TGEOS accurately predicted the probability distribution of pollutant concentrations in key polluted areas under different emission scenarios, along with potential extreme pollution events, with the probability distribution curves fitted from TGEOS predictions closely matching the corresponding GC curves. In addition, a comparison with traditional machine learning models reveals that TGEOS, built on the Transformer framework, demonstrates superior performance in air quality modeling, with correlation coefficients larger than 0.98 and 0.97 for $PM_{2.5}$ and O_3 predictions, respectively. Consequently, TGEOS offers more accurate and comprehensive predictive capabilities than alternative models and methods.

The TGEOS model still have some limitations to be improved. Firstly, it should be noted that the predictions generated by TGEOS remain incapable of accurately representing actual air pollutant concentrations, even though TGEOS is highly consistent with GEOS-Chem, since systematic biases have been demonstrated to exist within GEOS-Chem itself (Travis and Jacob, 2019; Miao et al., 2020). Therefore, correcting errors in TEGOS based on near-real observations or reanalysis data is of paramount importance and constitutes a priority for our subsequent research. Additionally, due to the considerable effect of meteorological conditions on the generation (Shi et al., 2020), spatiotemporal patterns (Zhang et al., 2013; Chen et al., 2020), and concentration levels (Wang et al., 2019) of $PM_{2.5}$ and O_3 concentrations, and meteorological conditions other than 2017 are not considered in this study. Consequently, there is also a need to incorporate various climate scenarios that represent meteorological variations to enhance the TGEOS's predictive capability regarding future air quality under more complex scenarios with variations in emissions and meteorology.

Code and data availability.

https://doi.org/10.5194/egusphere-2025-2186
Preprint. Discussion started: 28 May 2025

The GEOS-Chem v14.2.2 source code is archived on Zenodo (https://doi.org/10.5281/zenodo.10034814, The International GEOS-Chem User Community, 2023). The Python source codes of TGEOS v1.0 and two ML models are archived on Zenodo (https://doi.org/10.5281/zenodo.15422797, Li, 2025).

Author contributions.

JJ conceived the study and designed TGEOS v1.0. DL develop the model and multi-scenario dataset. HL provided ideas for the model. All authors contribute to writing the paper.

Acknowledgements. This work is supported by the National Natural Science Foundation of China (Grant No.42475150).

Competing interests

The authors declare that they have no conflict of interest.

https://doi.org/10.5194/egusphere-2025-2186
Preprint. Discussion started: 28 May 2025

References

Al-Kindi, S. G., Brook, R. D., Biswal, S., and Rajagopalan, S.: Environmental determinants of cardiovascular disease: lessons learned from air pollution, Nature Reviews Cardiology, 17, 656–672, 2020.

Bell, M. L., McDermott, A., Zeger, S. L., Samet, J. M., and Dominici, F.: Ozone and short-term mortality in 95 US urban communities, 1987-2000, Jama, 292, 2372–2378, 2004.

Bi, K., Xie, L., Zhang, H., Chen, X., Gu, X., and Tian, Q.: Pangu-weather: A 3d high-resolution model for fast and accurate global weather forecast, arXiv preprint arXiv:2211.02556, 2022.

Bond, T. C., Bhardwaj, E., Dong, R., Jogani, R., Jung, S., Roden, C., Streets, D. G., and Trautmann, N. M.: Historical emissions of black and organic carbon aerosol from energy-related combustion, 1850–2000, Global biogeochemical cycles, 21, 2007.

Box, G. E. and Draper, N. R.: Response surfaces, Mixtures, and Ridge Analyses, 649, 2007.

Burke, M., Childs, M. L., de la Cuesta, B., Qiu, M., Li, J., Gould, C. F., Heft-Neal, S., and Wara, M.: The contribution of wildfire to PM2. 5 trends in the USA, Nature, 622, 761–766, 2023.

Castruccio, S., McInerney, D. J., Stein, M. L., Crouch, F. L., Jacob, R. L., and Moyer, E. J.: Statistical emulation of climate model projections based on precomputed GCM runs, Journal of Climate, 27, 1829–1844, 2014.

Che, W., Zheng, J., Wang, S., Zhong, L., and Lau, A.: Assessment of motor vehicle emission control policies using Model-3/CMAQ model for the Pearl River Delta region, China, Atmospheric Environment, 45, 1740–1751, 2011.

Chen, C., Li, T., Sun, Q., Shi, W., He, M. Z., Wang, J., Liu, J., Zhang, M., Jiang, Q., Wang, M., et al.: Short-term exposure to ozone and cause-specific mortality risks and thresholds in China: Evidence from nationally representative data, 2013-2018, Environment International, 171, 107 666, 2023a.

Chen, K., Han, T., Gong, J., Bai, L., Ling, F., Luo, J.-J., Chen, X., Ma, L., Zhang, T., Su, R., et al.: Fengwu: Pushing the skillful global medium-range weather forecast beyond 10 days lead, arXiv preprint arXiv:2304.02948, 2023b.

Chen, L., Zhong, X., Zhang, F., Cheng, Y., Xu, Y., Qi, Y., and Li, H.: FuXi: A cascade machine learning forecasting system for 15-day global weather forecast, npj Climate and Atmospheric Science, 6, 190, 2023c.

Chen, S., Zhang, X., Lin, J., Huang, J., Zhao, D., Yuan, T., Huang, K., Luo, Y., Jia, Z., Zang, Z., et al.: Fugitive road dust PM2. 5 emissions and their potential health impacts, Environmental Science & Technology, 53, 8455–8465, 2019.

Chen, Z., Chen, D., Zhao, C., Kwan, M.-p., Cai, J., Zhuang, Y., Zhao, B., Wang, X., Chen, B., Yang, J., et al.: Influence of meteorological conditions on PM2. 5 concentrations across China: A review of methodology and mechanism, Environment international, 139, 105 558, 2020.

Cheng, J., Su, J., Cui, T., Li, X., Dong, X., Sun, F., Yang, Y., Tong, D., Zheng, Y., Li, Y., Li, J., Zhang, Q., and He, K.: Dominant role of emission reduction in $PM_{2.5}$ air quality improvement in Beijing during 2013–2017: a model-based decomposition analysis, Atmospheric Chemistry and Physics, 19, 6125–6146, https://doi.org/10.5194/acp-19-6125-2019, 2019.

Cheng, J., Tong, D., Liu, Y., Yu, S., Yan, L., Zheng, B., Geng, G., He, K., and Zhang, Q.: Comparison of current and future PM2. 5 air quality in China under CMIP6 and DPEC emission scenarios, Geophysical Research Letters, 48, e2021GL093 197, 2021.

Cheng, J., Tong, D., Liu, Y., Geng, G., Davis, S. J., He, K., and Zhang, Q.: A synergistic approach to air pollution control and carbon neutrality in China can avoid millions of premature deaths annually by 2060, One Earth, 6, 978–989, 2023.

CSC: Air pollution prevention and control action plan, https://www.gov.cn/zwgk/2013-09/12/content_2486773.htm, 2013.

https://doi.org/10.5194/egusphere-2025-2186
Preprint. Discussion started: 28 May 2025

CSC: Three-Year Action Plan for Winning the Blue Sky Defense Battle, https://english.mee.gov.cn/News_service/news_release/201807/t20180713_446624.shtml, 2018.

Devlin, J.: Bert: Pre-training of deep bidirectional transformers for language understanding, arXiv preprint arXiv:1810.04805, 2018.

EPA, U.: Technical Support Document for the Proposed PM NAAQS Rule: Response Surface Modeling, 2006.

Fang, L., Jin, J., Segers, A., Liao, H., Li, K., Xu, B., Han, W., Pang, M., and Lin, H. X.: A gridded air quality forecast through fusing site-available machine learning predictions from RFSML v1. 0 and chemical transport model results from GEOS-Chem v13. 1.0 using the ensemble Kalman filter, Geoscientific Model Development, 16, 4867–4882, 2023.

Fuller, R., Landrigan, P. J., Balakrishnan, K., Bathan, G., Bose-O'Reilly, S., Brauer, M., Caravanos, J., Chiles, T., Cohen, A., Corra, L., et al.: Pollution and health: a progress update, The Lancet Planetary Health, 6, e535–e547, 2022.

Gelaro, R., McCarty, W., Suárez, M. J., Todling, R., Molod, A., Takacs, L., Randles, C. A., Darmenov, A., Bosilovich, M. G., Reichle, R., et al.: The modern-era retrospective analysis for research and applications, version 2 (MERRA-2), Journal of climate, 30, 5419–5454, 2017.

Geng, G., Liu, Y., Liu, Y., Liu, S., Cheng, J., Yan, L., Wu, N., Hu, H., Tong, D., Zheng, B., et al.: Efficacy of China's clean air actions to tackle PM2. 5 pollution between 2013 and 2020, Nature Geoscience, pp. 1–8, 2024.

Gong, C., Liao, H., Zhang, L., Yue, X., Dang, R., and Yang, Y.: Persistent ozone pollution episodes in North China exacerbated by regional transport, Environmental pollution, 265, 115 056, 2020.

Guo, B., Wang, Y., Zhang, X., Che, H., Zhong, J., Chu, Y., and Cheng, L.: Temporal and spatial variations of haze and fog and the characteristics of PM2. 5 during heavy pollution episodes in China from 2013 to 2018, Atmospheric Pollution Research, 11, 1847–1856, 2020.

Han, H., Zhang, L., Wang, X., and Lu, X.: Contrasting domestic and global impacts of emission reductions in China on tropospheric ozone, Journal of Geophysical Research: Atmospheres, 129, e2024JD041 453, 2024.

Hoesly, R. M., Smith, S. J., Feng, L., Klimont, Z., Janssens-Maenhout, G., Pitkanen, T., Seibert, J. J., Vu, L., Andres, R. J., Bolt, R. M., et al.: Historical (1750–2014) anthropogenic emissions of reactive gases and aerosols from the Community Emissions Data System (CEDS), Geoscientific Model Development, 11, 369–408, 2018.

Hu, L., Jacob, D. J., Liu, X., Zhang, Y., Zhang, L., Kim, P. S., Sulprizio, M. P., and Yantosca, R. M.: Global budget of tropospheric ozone: Evaluating recent model advances with satellite (OMI), aircraft (IAGOS), and ozonesonde observations, Atmospheric Environment, 167, 323–334, 2017.

Hu, W., Zhao, Y., Lu, N., Wang, X., Zheng, B., Henze, D. K., Zhang, L., Fu, T.-M., and Zhai, S.: Changing responses of PM2. 5 and ozone to source emissions in the Yangtze River Delta using the adjoint model, Environmental Science & Technology, 58, 628–638, 2023.

Huang, L., Liu, S., Yang, Z., Xing, J., Zhang, J., Bian, J., Li, S., Sahu, S. K., Wang, S., and Liu, T.-Y.: Exploring deep learning for air pollutant emission estimation, Geoscientific Model Development Discussions, 2021, 1–22, 2021.

Jin, J., Fang, L., Li, B., Liao, H., Wang, Y., Han, W., Li, K., Pang, M., Wu, X., and Lin, H. X.: 4DEnVar-based inversion system for ammonia emission estimation in China through assimilating IASI ammonia retrievals, Environmental Research Letters, 18, 034 005, 2023.

Kelp, M. M., Jacob, D. J., Lin, H., and Sulprizio, M. P.: An online-learned neural network chemical solver for stable long-term global simulations of atmospheric chemistry, Journal of Advances in Modeling Earth Systems, 14, e2021MS002 926, 2022.

Kingma, D. P.: Adam: A method for stochastic optimization, arXiv preprint arXiv:1412.6980, 2014.

Le, T., Wang, Y., Liu, L., Yang, J., Yung, Y. L., Li, G., and Seinfeld, J. H.: Unexpected air pollution with marked emission reductions during the COVID-19 outbreak in China, Science, 369, 702–706, 2020.

https://doi.org/10.5194/egusphere-2025-2186
Preprint. Discussion started: 28 May 2025

LeCun, Y., Bengio, Y., and Hinton, G.: Deep learning, nature, 521, 436–444, 2015.

Lelieveld, J., Evans, J. S., Fnais, M., Giannadaki, D., and Pozzer, A.: The contribution of outdoor air pollution sources to premature mortality on a global scale, Nature, 525, 367–371, 2015.

Li, D.: Python source code of TGEOS v1.0, https://doi.org/10.5281/zenodo.15422797, 2025.

Li, D., Wu, Q., Cheng, H., Feng, J., Li, D., Wang, Y., Cao, K., and Wang, L.: Numerical study of the future PM2. 5 concentration under climate change and Best-Health-Effect (BHE) scenario, Environmental Pollution, p. 124391, 2024.

Li, J., Dai, Y., Zhu, Y., Tang, X., Wang, S., Xing, J., Zhao, B., Fan, S., Long, S., and Fang, T.: Improvements of response surface modeling with self-adaptive machine learning method for PM2. 5 and O3 predictions, Journal of Environmental Management, 303, 114 210, 2022.

Li, M., Liu, H., Geng, G., Hong, C., Liu, F., Song, Y., Tong, D., Zheng, B., Cui, H., Man, H., et al.: Anthropogenic emission inventories in China: a review, National Science Review, 4, 834–866, 2017.

Liang, Y., Xia, Y., Ke, S., Wang, Y., Wen, Q., Zhang, J., Zheng, Y., and Zimmermann, R.: Airformer: Predicting nationwide air quality in china with transformers, in: Proceedings of the AAAI Conference on Artificial Intelligence, vol. 37, pp. 14 329–14 337, 2023.

Liu, C., Zhang, H., Cheng, Z., Shen, J., Zhao, J., Wang, Y., Wang, S., and Cheng, Y.: Emulation of an atmospheric gas-phase chemistry solver through deep learning: Case study of Chinese Mainland, Atmospheric Pollution Research, 12, 101 079, 2021.

Lu, X., Zhang, L., Wang, X., Gao, M., Li, K., Zhang, Y., Yue, X., and Zhang, Y.: Rapid increases in warm-season surface ozone and resulting health impact in China since 2013, Environmental Science & Technology Letters, 7, 240–247, 2020a.

Lu, X., Zhang, L., Wu, T., Long, M. S., Wang, J., Jacob, D. J., Zhang, F., Zhang, J., Eastham, S. D., Hu, L., Zhu, L., Liu, X., and Wei, M.: Development of the global atmospheric chemistry general circulation model BCC-GEOS-Chem v1.0: model description and evaluation, Geoscientific Model Development, 13, 3817–3838, https://doi.org/10.5194/gmd-13-3817-2020, 2020b.

Masmoudi, S., Elghazel, H., Taieb, D., Yazar, O., and Kallel, A.: A machine-learning framework for predicting multiple air pollutants' concentrations via multi-target regression and feature selection, Science of the Total Environment, 715, 136 991, 2020.

McDuffie, E. E., Martin, R. V., Spadaro, J. V., Burnett, R., Smith, S. J., O'Rourke, P., Hammer, M. S., van Donkelaar, A., Bindle, L., Shah, V., et al.: Source sector and fuel contributions to ambient PM2. 5 and attributable mortality across multiple spatial scales, Nature communications, 12, 1–12, 2021.

Miao, R., Chen, Q., Zheng, Y., Cheng, X., Sun, Y., Palmer, P. I., Shrivastava, M., Guo, J., Zhang, Q., Liu, Y., et al.: Model bias in simulating major chemical components of PM 2.5 in China, Atmospheric Chemistry and Physics, 20, 12 265–12 284, 2020.

Nair, V. and Hinton, G. E.: Rectified linear units improve restricted boltzmann machines, in: Proceedings of the 27th international conference on machine learning (ICML-10), pp. 807–814, 2010.

Narayanan, D., Shoeybi, M., Casper, J., LeGresley, P., Patwary, M., Korthikanti, V., Vainbrand, D., Kashinkunti, P., Bernauer, J., Catanzaro, B., et al.: Efficient large-scale language model training on gpu clusters using megatron-lm, in: Proceedings of the International Conference for High Performance Computing, Networking, Storage and Analysis, pp. 1–15, 2021.

Organization, W. H. et al.: Air pollution: The invisible health threat, World Health Organization: Geneva, Switzerland, 2023.

Qiao, X., Yuan, Y., Tang, Y., Ying, Q., Guo, H., Zhang, Y., and Zhang, H.: Revealing the origin of fine particulate matter in the Sichuan Basin from a source-oriented modeling perspective, Atmospheric Environment, 244, 117 896, 2021.

Rodríguez, S. and López-Darias, J.: Extreme Saharan dust events expand northward over the Atlantic and Europe, prompting record-breaking PM10 and PM2. 5 episodes, Atmospheric Chemistry and Physics, 24, 12 031–12 053, 2024.

Salman, A. K., Choi, Y., Park, J., Mousavinezhad, S., Payami, M., Momeni, M., and Ghahremanloo, M.: Deep learning based emulator for simulating CMAQ surface NO2 levels over the CONUS, Atmospheric Environment, 316, 120 192, 2024.

https://doi.org/10.5194/egusphere-2025-2186
Preprint. Discussion started: 28 May 2025

Santner, T., Williams, B., and Notz, W.: The design and analysis of computer experiments springer-verlag, New York. 283pp, 25, 2003.

Seinfeld, J. H. and Pandis, S. N.: Atmospheric chemistry and physics: from air pollution to climate change, John Wiley & Sons, 2016.

Shi, Z., Huang, L., Li, J., Ying, Q., Zhang, H., and Hu, J.: Sensitivity analysis of the surface ozone and fine particulate matter to meteorological parameters in China, Atmospheric Chemistry and Physics, 20, 13 455–13 466, 2020.

Silver, B., Reddington, C., Arnold, S., and Spracklen, D.: Substantial changes in air pollution across China during 2015–2017, Environmental Research Letters, 13, 114 012, 2018.

Taylor, K. E.: Taylor diagram primer, Work. Pap, pp. 1–4, 2005.

The International GEOS-Chem User Community: geoschem/GCClassic: GCClassic 14.2.2, https://doi.org/10.5281/zenodo.10034814, 2023.

Thompson, T. M. and Selin, N. E.: Influence of air quality model resolution on uncertainty associated with health impacts, Atmospheric Chemistry and Physics, 12, 9753–9762, 2012.

Thunis, P., Clappier, A., Beekmann, M., Putaud, J. P., Cuvelier, C., Madrazo, J., and de Meij, A.: Non-linear response of PM 2.5 to changes in NO x and NH 3 emissions in the Po basin (Italy): Consequences for air quality plans, Atmospheric Chemistry and Physics, 21, 9309–9327, 2021.

Tian, F., Qi, J., Qian, Z., Li, H., Wang, L., Wang, C., Geiger, S. D., McMillin, S. E., Yin, P., Lin, H., et al.: Differentiating the effects of air pollution on daily mortality counts and years of life lost in six Chinese megacities, Science of the Total Environment, 827, 154 037, 2022.

Tong, D., Cheng, J., Liu, Y., Yu, S., Yan, L., Hong, C., Qin, Y., Zhao, H., Zheng, Y., Geng, G., et al.: Dynamic projection of anthropogenic emissions in China: methodology and 2015–2050 emission pathways under a range of socio-economic, climate policy, and pollution control scenarios, Atmospheric Chemistry and Physics, 20, 5729–5757, 2020.

Travis, K. R. and Jacob, D. J.: Systematic bias in evaluating chemical transport models with maximum daily 8 h average (MDA8) surface ozone for air quality applications: a case study with GEOS-Chem v9. 02, Geoscientific Model Development, 12, 3641–3648, 2019.

Vaswani, A.: Attention is all you need, Advances in Neural Information Processing Systems, 2017.

Wang, F., Han, X., Xie, H., Gao, Y., Guan, X., and Zhang, M.: Investigating trends and causes of simultaneous high pollution from PM2. 5 and ozone in China, 2015–2023, Atmospheric Pollution Research, p. 102351, 2024.

Wang, P., Guo, H., Hu, J., Kota, S. H., Ying, Q., and Zhang, H.: Responses of PM2. 5 and O3 concentrations to changes of meteorology and emissions in China, Science of the Total Environment, 662, 297–306, 2019.

Wang, S., Xing, J., Jang, C., Zhu, Y., Fu, J. S., and Hao, J.: Impact assessment of ammonia emissions on inorganic aerosols in East China using response surface modeling technique, Environmental science & technology, 45, 9293–9300, 2011.

Wang, T., Xue, L., Brimblecombe, P., Lam, Y. F., Li, L., and Zhang, L.: Ozone pollution in China: A review of concentrations, meteorological influences, chemical precursors, and effects, Science of the Total Environment, 575, 1582–1596, 2017.

Wang, X., Fu, T.-M., Zhang, L., Cao, H., Zhang, Q., Ma, H., Shen, L., Evans, M. J., Ivatt, P. D., Lu, X., et al.: Sensitivities of ozone air pollution in the Beijing–Tianjin–Hebei area to local and upwind precursor emissions using adjoint modeling, Environmental Science & Technology, 55, 5752–5762, 2021.

Wang, Y., Zhao, Y., Liu, Y., Jiang, Y., Zheng, B., Xing, J., Liu, Y., Wang, S., and Nielsen, C. P.: Sustained emission reductions have restrained the ozone pollution over China, Nature Geoscience, 16, 967–974, 2023.

Wei, T., Chen, C., Yang, Y., Li, L., Wang, J., Ye, M., Kan, H., Yang, D., Song, Y., Cai, J., et al.: Associations between short-term exposure to ambient air pollution and lung function in adults, Journal of exposure science & environmental epidemiology, 34, 886–894, 2024.

Wei, W., Li, Y., Ren, Y., Cheng, S., and Han, L.: Sensitivity of summer ozone to precursor emission change over Beijing during 2010–2015: A WRF-Chem modeling study, Atmospheric environment, 218, 116 984, 2019.

https://doi.org/10.5194/egusphere-2025-2186
Preprint. Discussion started: 28 May 2025

Xiao, Q., Geng, G., Xue, T., Liu, S., Cai, C., He, K., and Zhang, Q.: Tracking PM2. 5 and O3 pollution and the related health burden in China 2013–2020, Environmental science & technology, 56, 6922–6932, 2021.

Xing, J., Wang, S., Jang, C., Zhu, Y., and Hao, J.: Nonlinear response of ozone to precursor emission changes in China: a modeling study using response surface methodology, Atmospheric Chemistry and Physics, 11, 5027–5044, 2011.

Xing, J., Wang, S., Zhao, B., Wu, W., Ding, D., Jang, C., Zhu, Y., Chang, X., Wang, J., Zhang, F., et al.: Quantifying nonlinear multiregional contributions to ozone and fine particles using an updated response surface modeling technique, Environmental science & technology, 51, 11 788–11 798, 2017.

Xing, J., Ding, D., Wang, S., Zhao, B., Jang, C., Wu, W., Zhang, F., Zhu, Y., and Hao, J.: Quantification of the enhanced effectiveness of NO x control from simultaneous reductions of VOC and NH 3 for reducing air pollution in the Beijing–Tianjin–Hebei region, China, Atmospheric Chemistry and Physics, 18, 7799–7814, 2018.

Xing, J., Zheng, S., Ding, D., Kelly, J. T., Wang, S., Li, S., Qin, T., Ma, M., Dong, Z., Jang, C., et al.: Deep learning for prediction of the air quality response to emission changes, Environmental science & technology, 54, 8589–8600, 2020.

Yan, Y., Zhou, Y., Kong, S., Lin, J., Wu, J., Zheng, H., Zhang, Z., Song, A., Bai, Y., Ling, Z., et al.: Effectiveness of emission control in reducing PM 2.5 pollution in central China during winter haze episodes under various potential synoptic controls, Atmospheric Chemistry and Physics, 21, 3143–3162, 2021.

Yang, S. and Wu, H.: A novel PM2. 5 concentrations probability density prediction model combines the least absolute shrinkage and selection operator with quantile regression, Environmental Science and Pollution Research, 29, 78 265–78 291, 2022.

Zeng, X., Gao, Y., Wang, Y., Ma, M., Zhang, J., and Sheng, L.: Characterizing the distinct modulation of future emissions on summer ozone concentrations between urban and rural areas over China, Science of the Total Environment, 820, 153 324, 2022.

Zhang, J., Gao, Y., Luo, K., Leung, L. R., Zhang, Y., Wang, K., and Fan, J.: Impacts of compound extreme weather events on ozone in the present and future, Atmospheric Chemistry and Physics, 18, 9861–9877, 2018.

Zhang, X., Xiao, X., Wang, F., Brasseur, G., Chen, S., Wang, J., and Gao, M.: Observed sensitivities of PM2. 5 and O3 extremes to meteorological conditions in China and implications for the future, Environment International, 168, 107 428, 2022a.

Zhang, Y., Mao, H., Ding, A., Zhou, D., and Fu, C.: Impact of synoptic weather patterns on spatio-temporal variation in surface O3 levels in Hong Kong during 1999–2011, Atmospheric Environment, 73, 41–50, 2013.

Zhang, Y., Gao, J., Zhu, Y., Liu, Y., Li, H., Yang, X., Zhong, X., Zhao, M., Wang, W., Che, F., et al.: Evolution of ozone formation sensitivity during a persistent regional ozone episode in Northeastern China and its implication for a control strategy, Environmental Science & Technology, 58, 617–627, 2023.

Zhang, Z., Yan, Y., Kong, S., Deng, Q., Qin, S., Yao, L., Zhao, T., and Qi, S.: Benefits of refined NH3 emission controls on PM2. 5 mitigation in Central China, Science of the Total Environment, 814, 151 957, 2022b.

Zhao, B., Wang, S., Xing, J., Fu, K., Fu, J., Jang, C., Zhu, Y., Dong, X., Gao, Y., Wu, W., et al.: Assessing the nonlinear response of fine particles to precursor emissions: development and application of an extended response surface modeling technique v1. 0, Geoscientific Model Development, 8, 115–128, 2015.

Zhao, S., Feng, T., Xiao, W., Zhao, S., and Tie, X.: Weather-Climate Anomalies and Regional Transport Contribute to Air Pollution in Northern China During the COVID-19 Lockdown, Journal of Geophysical Research: Atmospheres, 127, e2021JD036 345, 2022.

Zheng, B., Zhang, Q., Geng, G., Chen, C., Shi, Q., Cui, M., Lei, Y., and He, K.: Changes in China's anthropogenic emissions and air quality during the COVID-19 pandemic in 2020, Earth System Science Data, 13, 2895–2907, 2021.

https://doi.org/10.5194/egusphere-2025-2186
Preprint. Discussion started: 28 May 2025

660 Zhou, H., Zhang, S., Peng, J., Zhang, S., Li, J., Xiong, H., and Zhang, W.: Informer: Beyond efficient transformer for long sequence time-series forecasting, in: Proceedings of the AAAI conference on artificial intelligence, vol. 35, pp. 11 106–11 115, 2021.

Zhou, S., Wang, W., Zhu, L., Qiao, Q., and Kang, Y.: Deep-learning architecture for PM2. 5 concentration prediction: A review, Environmental Science and Ecotechnology, p. 100400, 2024.